L.M. Gordon
K.Y.C. Lee
M.M. Lipp
J.A. Zasadzinski
F.J. Walther
M.A. Sherman
A.J. Waring

Conformational mapping of the N-terminal segment of surfactant protein B in lipid using ^{13}C-enhanced Fourier transform infrared spectroscopy

Authors' affiliations:
L.M. Gordon, F.J. Walther and A.J. Waring, Department of Pediatrics, Martin Luther King, Jr./Drew University Medical Center and UCLA, Los Angeles, CA, USA.

K.Y.C. Lee, Institute of Biophysical Dynamics and Department of Chemistry, The University of Chicago, Chicago, IL, USA.

M.M. Lipp, Advanced Inhalation Research, Cambridge, MA, USA.

J.A. Zasadzinski, Department of Chemical Engineering, UCSB, Santa Barbara, CA, USA.

M.A. Sherman, Physical Biochemistry Section, Division of Biology, Beckman Research Institute, City of Hope Medical Center, Duarte, CA, USA.

Correspondence to:
Dr *A. J. Waring*
Bldg RB-1
Harbor UCLA
Research and Education Instituite
1124 West Carson Street
Torrance
CA 90502-2064
USA
Tel.: 1-323-563-5957
Fax: 1-310-668-3407
E-mail: awaring@ucla.edu

Dates:
Received 27 July 1999
Revised 21 September 1999
Accepted 15 November 1999

To cite this article:
Gordon, L.M., Lee, K.Y.C., Lipp, M.M., Zasadzinski, J.A., Walther, F.J., Sherman, M.A. & Waring, A.J. Conformational mapping of the N-terminal segment of surfactant protein B in lipid using ^{13}C-enhanced Fourier transform infrared spectroscopy.
J. Peptide Res., 2000, **55**, 330–347.

ISSN 1397-002X

Key words: CD spectroscopy; isotope-enhanced FTIR spectroscopy; lung surfactant protein; peptide; saposin; secondary structure

Abstract: Synthetic peptides based on the N-terminal domain of human surfactant protein B (SP-B_{1-25}; 25 amino acid residues; NH_2-FPIPLPYCWLCRALIKRIQAMIPKG) retain important lung activities of the full-length, 79-residue protein. Here, we used physical techniques to examine the secondary conformation of SP-B_{1-25} in aqueous, lipid and structure-promoting environments. Circular dichroism and conventional, ^{12}C-Fourier transform infrared (FTIR) spectroscopy each indicated a predominate α-helical conformation for SP-B_{1-25} in phosphate-buffered saline, liposomes of 1-palmitoyl-2-oleoyl phosphatidylglycerol and the structure-promoting solvent hexafluoroisopropanol; FTIR spectra also showed significant β- and random conformations for peptide in these three environments. In further experiments designed to map secondary structure to specific residues, isotope-enhanced FTIR spectroscopy was performed with 1-palmitoyl-2-oleoyl phosphatidylglycerol liposomes and a suite of SP-B_{1-25} peptides labeled with ^{13}C-carbonyl groups at either single or multiple sites. Combining these ^{13}C-enhanced FTIR results with energy minimizations and molecular simulations indicated the following model for SP-B_{1-25} in 1-palmitoyl-2-oleoyl phosphatidylglycerol: β-sheet (residues 1–6), α-helix (residues 8–22) and random (residues 23–25) conformations. Analogous structural motifs are observed in the corresponding homologous N-terminal regions of several proteins that also share the 'saposin-like' (i.e. 5-helix bundle) folding pattern of full-length, human SP-B. In future studies, ^{13}C-enhanced FTIR spectroscopy and energy minimizations may be of general use in defining backbone conformations at amino acid resolution, particularly for peptides or proteins in membrane environments.

Abbreviations: PBS, phosphate-buffered saline; HFIP, hexafluoroisopropanol; TFE, trifluoroethanol; SDS, sodium dodecyl sulfate; Tanaka lipids, dipalmitoylphosphatidylcholine/unsaturated phosphatidylglycerol/palmitic acid (66:22:9, wt%); ATR, attenuated-total-reflectance; FTIR, Fourier-transform infrared spectroscopy; ^{13}C-FTIR, isotopically enhanced ^{13}C-Fourier transform infrared spectroscopy; ^{12}C-FTIR, conventional FTIR spectroscopy on native peptides; CD, circular dichroism; 2D-NMR, two-dimensional nuclear magnetic resonance; ESR, electron spin resonance; POPG, 1-palmitoyl-2-oleoyl phosphatidylglycerol; SP-B, human surfactant protein B, residues 1–79; SP-B_{1-25}, N-terminal peptide of human surfactant protein B, residues 1–25; SP-B_{1-9}, truncated N-terminal segment of SP-B, residues 1–9; SP-B_{8-25}, truncated N-terminal segment of SP-B, residues 8–25; SP-B_{11-25}, truncated N-terminal segment of SP-B, residues 11–25; SP-C, surfactant protein C; P/L, peptide to lipid molar ratio; LUV, large unilamellar vesicle liposomes; HPLC, high-performance liquid chromatography.

Surfactant protein B (SP-B) is a small (amino acid residues 1–79; $M_r \approx 8700$), lipid-associating protein found in mammalian lung surfactant (1), with a conserved antigenic structure of ≈ 300 million years [2]. An important role for SP-B in lung function is indicated by previous findings showing that mutations in the SP-B gene cause severe lung disease (3, 4); moreover, preparations containing either synthetic, full-length SP-B (5) or synthetic peptides representing N-terminal and C-terminal domains of SP-B (6) improve oxygenation and lung compliance in surfactant-deficient animal models. Synthetic or native full-length SP-B exhibits substantial antimicrobial activity *in vitro* (7, 8), and may participate, along with lung surfactant proteins A and D, as a first line of defense against pathogenic bacteria and viruses (9). SP-B is encoded on chromosome two and synthesized in type II pneumocytes (1). After being processed from the larger preproprotein (10), mature SP-B is very hydrophobic and partitions into the chloroform phase with surfactant lipids when isolated from lung lavage using the Folch *et al*. (11) extraction procedure. Plasma desorption mass spectral analysis of native SP-B indicates that, while the protein has no post-translational modifications, each SP-B monomer contains three intramolecular disulfide bridges, linking Cys^{8} to Cys^{77}, Cys^{11} to Cys^{71} and Cys^{35} to Cys^{46} (12). The predominate molecular species of SP-B is a disulfide-linked (through Cys^{48}) homodimer, although variable amounts of monomer are also seen in samples isolated from lung surfactant.

The polypeptide motif of monomeric SP-B, characterized by six Cys residues paired as disulfides and periodic hydrophobic residues, belongs to a class of 'saposin-like' proteins that also includes saposins A–D, sulfated glycoprotein-I, acid sphingomyelinase, acyloxyacyl hydrolase, *Entamoeba histolytica* pore-forming peptides (amoebapores), plant aspartic proteases and NK-lysin (10, 13–15). SP-B, as well as other proteins of the saposin family, uniformly exhibits high levels of α-helix (13, 14, 16–19), suggesting that this motif plays a critical structural role. Based on the crystallographic structure of the related hemerythrin (13, 20) and the 2D-NMR structure of NK-lysin (21), the saposin-fold is apparently characterized by amphipathic α-helices with hydrophilic residues facing the solvent, and hydrophobic side-chains forming a core stabilized by intramolecular disulfide bonds.

Given the critical *in vivo* role of SP-B in lung function, it is of interest that numerous actions of the full-length protein on surfactant lipids are mimicked by a synthetic peptide representing the N-terminal domain of SP-B (i.e. SP-B_{1-25}; residues 1–25; Table 1). Both SP-B and positively charged SP-B_{1-25} increase the collapse pressure of surfactant lipid monolayers containing palmitic acid; this suggests that the cationic N-terminus of SP-B interacts with anionic lipids to remove the driving force for lipid squeeze-out from the surface film (22, 23). Another indication of specific interactions of proteins with lipids is the insertion of the protein into monolayers at varying surface pressures. The critical insertion pressure, an index of the degree of protein association with lipid films and membrane systems, is very high for both SP-B_{1-25} and the parent SP-B (17, 24, 25). Furthermore, full-length SP-B and SP-B_{1-25} each similarly induce a coexistence of buckled and flat monolayers when added to surfactant lipids, which may participate in the reduction of surface tension and the enhancement of respreadability of the surfactant monolayer (26). Finally, initial studies indicate that SP-B_{1-25} has been shown to mediate lipid–vesicle mixing (27), as does the native SP-B (10, 28, 29).

In view of the likely participation of the N-terminal region of SP-B in key surfactant activities, it is important to elucidate the structure of this domain in lipid environments. Earlier theoretical analysis of the primary sequence of SP-B, using the hydrophobic moment algorithm or Chou-Fasman secondary structure predictions, suggested both a N-terminal β-turn (residues 6–9; Table 1) (30) and an α-helical segment (residues 10–22) (6, 24, 31, 32). Physical experiments on synthetic peptides based on the SP-B N-terminus have also been performed to more directly assign secondary

Table 1. **Amino acid sequences[a] of native and 'cassette' ^{13}C-labeled N-terminal human SP-B_{1-25} peptides**

SP-B_{1-25} [N-terminal segment of SP-B, residues 1–25]
NH_2FPIPLPYCWLCRALIKRIQAMIPKGCOOH
1 25
SP-B_{1-25} (F1/I3/L5) [SP-B_{1-25}, ^{13}C-carbonyl labeled at Phe^{1}, Ile^{3}, Leu^{5}]
NH_2 (F*)P(I*)P(L*)PYCWLCRALIKRIQAMIPKGCOOH
SP-B_{1-25} (A8/A11) [SP-B_{1-25} variant, ^{13}C-carbonyl labeled at Ala^{8}, Ala^{11}]
NH_2FPIPLPY(A*)WL(A*)RALIKRIQAMIPKGCOOH
SP-B_{1-25} (L10/A13/L14) [SP-B_{1-25}, ^{13}C-carbonyl labeled at Leu^{10}, Ala^{13}, Leu^{14}]
NH_2FPIPLPYCW(L*)CR(A*)(L*)IKRIQAMIPKGCOOH
SP-B_{1-25} (I18/A20/I22) [SP-B_{1-25}, ^{13}C-carbonyl labeled at Ile^{18}, Ala^{20}, Ile^{22}]
NH_2FPIPLPYCWLCRALIKR(I*)Q(A*)M(I*)PKGCOOH

a. Amino acids are represented by one letter codes. The ^{13}C-carbonyl-labeled residues are indicated in parentheses with an asterisk.

conformations. Previous circular dichroism (CD) and Fourier transform infrared (FTIR) spectroscopy on SP-B_{1-25} in lipids or solvents that mimic membranes [e.g. methanol, trifluoroethanol (TFE)] indicated dominant helical content, with minor β- and disordered components (24, 33). Upon repeating these experiments with a series of truncated SP-B peptides in methanol, a structural model was developed indicating that residues 8–25 (Table 1) were largely α-helix, while residues 1–8 were primarily β-sheet and β-turn [33]. An earlier proton 2D-NMR study of the truncated peptide SP-B_{11-25}, suspended in the membrane mimics methanol or sodium dodecyl sulfate (SDS) similarly demonstrated α-helix for residues 14–21 (34). However, caution must be employed in extrapolating these structural findings using truncated N-terminal SP-B peptides to the corresponding conformation of SP-B_{1-25} in membrane lipids. Experiments using truncated peptides to localize conformations have inherent uncertainties, not only because shortened peptides may artificially fray at their unprotected N-terminal and C-terminal ends, but also because peptide conformations in membrane mimics (e.g. methanol, SDS) may not faithfully reflect structure in lipid environments. Accordingly, it is important to directly characterize the residue-specific conformation of SP-B_{1-25} in lipids using alternative methodologies.

Here, we study the structure of the N-terminal SP-B_{1-25} peptide in phosphate-buffered saline (PBS), the membrane mimic hexafluoroisopropanol (HFIP), or the lipid 1-palmitoyl-2-oleoyl phosphatidylglycerol (POPG) using CD and conventional ^{12}C-FTIR spectroscopy. Additional FTIR experiments were performed using site-directed, ^{13}C-labeled SP-B_{1-25} to assess the residue-specific conformations of peptide bound to POPG liposomes. Previous ^{13}C-labeled FTIR spectroscopic investigations have identified specific random, β-strand and β-turn structural domains in a soluble peptide (35), and also α-helical structure for discrete regions in the transmembrane domain of phospholamban (36). Here, isotope-labeled SP-B_{1-25} peptides were prepared, in which ^{13}C-carbonyl groups are introduced at various amino acids throughout the peptide. When suites of single and multiply ^{13}C-enhanced SP-B_{1-25} peptides were incorporated into POPG liposomes, the resulting FTIR spectra permitted the mapping of secondary conformation to individual amino acids. POPG liposomes were chosen to provide a homogenous lipid environment for SP-B_{1-25} incorporation not only because POPG is found at relatively high levels (≈ 22%) in lung surfactant preparations, such as Tanaka lipids [33], but also because SP-B_{1-25} is cationic and associates preferentially with the anionic lipids in surfactant dispersions (22, 24, 37).

Experimental Procedures

Materials

Peptide synthesis reagents including Fmoc amino acids and coupling solvents were obtained from Applied Biosystems. Deuterium was supplied by Aldrich Chemical Co. Fmoc ^{13}C-carbonyl leucine, isoleucine, alanine and glycine were purchased from Cambridge Isotope Laboratories. ^{13}C-carbonyl phenylalanine (Cambridge Isotope Laboratories) was converted to the Fmoc derivative by AnaSpec. POPG was obtained from Avanti Polar Lipids. All organic solvents used for sample synthesis, purification and preparation were HPLC grade or better.

Solid-phase peptide synthesis, purification and characterization

The native 25 amino acid, N-terminal domain of human surfactant protein B (SP-B_{1-25}; Table 1), and also the ^{13}C-enhanced SP-B_{1-25} analogs (Tables 1 and 2), were prepared using an ABI 431A peptide synthesizer, and purified as described previously (33). The expected molecular masses of SP-B_{1-25} and SP-B_{1-25} analogs were obtained by fast-atom bombardment and electrospray mass spectrometry (UCLA Center for Molecular and Medical Sciences Mass Spectrometry). Quantitative amino acid compositions for the peptides were determined at the UCLA Protein Microsequencing Facility.

Rationale for ^{13}C-site directed SP-B_{1-25} substitutions

To probe the secondary conformations within SP-B_{1-25}, FTIR spectroscopy was conducted here using two categories of site-directed, isotope-enhanced peptides. The first class involves the incorporation of ^{13}C-carbonyl groups into multiple, neighboring amino acid residues of synthetic SP-B_{1-25} peptides (Table 1). Separate peptides were synthesized with 'cassettes' of multiply ^{13}C-enhanced substitutions that were staggered to sequentially cover the peptide (Table 1). In earlier studies (35, 36), cassettes of similarly ^{13}C-enhanced peptides allowed local domain mapping of various secondary conformations (e.g. α-helix, β-sheet, β-turn, random). The rationale behind such experiments is that the secondary structure within a peptide usually extends over more than several adjacent residues (38). The second class involves peptides substituted with ^{13}C-carbonyl groups at single amino acid residues (Table 2). FTIR spectroscopic analysis of single-site ^{13}C-enhanced peptides may assign the secondary conformation to individual residues (36); in cases in which the labeled amino acid exhibits considerable flexibility, use of single-site ^{13}C-enhanced peptides may indicate multiple conformations that coexist simultaneously.

Most of the isotopically enhanced SP-B_{1-25} peptides in Table 1 [i.e. SP-B_{1-25} (F1/I3/L5), SP-B_{1-25} (L10/A13/L14) and SP-B_{1-25} (I18/A20/I22)] and Table 2 [i.e. SP-B_{1-25} (I15), SP-B_{1-25} (I18), SP-B_{1-25} (A20) and SP-B_{1-25} (G25)] share the same chemical composition as the native peptide. Since ^{13}C-carbonyl Cys is not available commercially, the local region of SP-B_{1-25} at Cys^{8} and Cys^{11} was probed by substituting these residues with ^{13}C-carbonyl Ala [i.e. SP-B_{1-25} (A8/A11) in Table 1 and SP-B_{1-25} (A8) and SP-B_{1-25} (A11) in Table 2]. Earlier studies (24) with a SP-B_{1-25} variant, in which Cys^{8} and Cys^{11} were replaced with alanine residues, showed that these substitutions did not perturb either peptide–lipid binding or the secondary conformation of the peptide when bound to lipids.

***Table 2*. Amino acid sequences[a] of native and single ^{13}C-labeled N-terminal human SP-B_{1-25} peptides**

SP-B_{1-25} [N-terminal segment of SP-B, residues 1–25]
NH_2FPIPLPYCWLCRALIKRIQAMIPKGCOOH
1 25
SP-B_{1-25} (A8) [SP-B_{1-25} variant, ^{13}C-carbonyl labeled at Ala^{8}]
NH_2FPIPLPY(A*)WLCRALIKRIQAMIPKGCOOH
SP-B_{1-25} (A11) [SP-B_{1-25} variant, ^{13}C-carbonyl labeled at Ala^{11}]
NH_2FPIPLPYCWL(A*)RALIKRIQAMIPKGCOOH
SP-B_{1-25} (I15) [SP-B_{1-25}, ^{13}C-carbonyl labeled at Ile^{15}]
NH_2FPIPLPYCWLCRAL(I*)KRIQAMIPKGCOOH
SP-B_{1-25} (I18) [SP-B_{1-25}, ^{13}C-carbonyl labeled at Ile^{18}]
NH_2FPIPLPYCWLCRALIKR(I*)QAMIPKGCOOH
SP-B_{1-25} (A20) [SP-B_{1-25}, ^{13}C-carbonyl labeled at Ala^{20}]
NH_2FPIPLPYCWLCRALIKRIQ(A*)MIPKGCOOH
SP-B_{1-25} (G25) [SP-B_{1-25}, ^{13}C-carbonyl labeled at Gly^{25}]
NH_2FPIPLPYCWLCRALIKRIQAMIPK(G*)COOH

a. Amino acids are represented by one letter codes. The ^{13}C-carbonyl-labeled residues are indicated in parentheses with an asterisk.

Liposome preparation

Large unilamellar vesicles (LUV) of POPG in PBS (500 nmoles lipid/mL) used for CD and FTIR spectroscopic studies were prepared by extrusion through polycarbonate membrane filters (39). A dry lipid film was hydrated with buffer-saline solution, followed by vortexing of the dispersion to form multilamellar vesicles. The suspension was freeze–thawed five times, and then extruded through 100-nm pore polycarbonate filters (Nuclepore Corp., Pleasanton, CA, USA) fives times using a LipoFast device (Avestin Inc., Ottawa, ON, Canada). The size distribution of extruded unilamellar vesicles was determined by dynamic light scattering with a Microtrac 9230 UPA ultrafine particle analyzer (Leeds and Northrup, St. Peterburg, FL, USA) (40). Extrusion through the 100-nm pore filters yielded a single population of POPG vesicles with a mean diameter of 95.8 nm and a standard deviation of 20.3 nm.

CD Spectroscopy

CD measurements were carried out using an AVIV 62DS spectropolarimeter (AVIV Associates), fitted with a thermoelectric temperature controller that maintained the sample temperature at 25°C (33, 41). Peptide solutions or peptide/liposome suspensions were measured in 0.1-mm light path demountable cells scanned from 250 to 185 nm at a rate of 10 nm/min and a sample interval of 0.2 nm. The instrument was routinely calibrated with (+)-10-camphorsulfonic acid (1 mg/mL) and a 1-mm path length cell (42), and the ellipticity expressed as the mean residue ellipticity, $[\Theta]_{MRE}$ (deg cm^2/dmol). Peptide sample concentrations were determined from quantitative amino acid analysis (UCLA Microsequencing Facility).

The α-helical structure of SP-B peptides in solvent or lipid environments was determined from CD spectra using the following methodology. The percentage of α-helix conformation in the peptide was first estimated using the

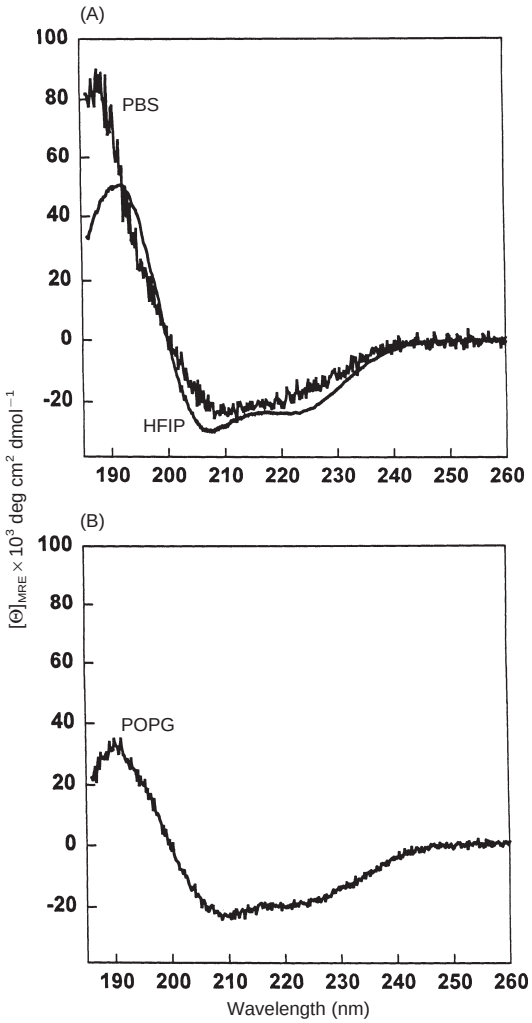

Figure 1. CD spectra of SP-B_{1-25} in solvents and POPG liposome dispersions, showing the mean residue ellipticities ($[\Theta]_{MRE} \times 10^3$ deg cm²/dmol). The optical pathlength was 1 mm and the temperature was 25°C. (A) SP-B_{1-25} was either suspended at 225 μM in PBS, pH 7.4, or 173 μM in HFIP/H_2O (7:3, v/v) with 10 mM phosphate, pH 7.4 (i.e. HFIP solution). (B) SP-B_{1-25} (220 μM) was added to POPG liposomes at an initial peptide/lipid (P/L) ratio of 1:70 suspended in PBS, pH 7.4. Peptide/liposomes were chromatographed to remove nonlipid associated SP-B_{1-25}, as described in Experimental procedures.

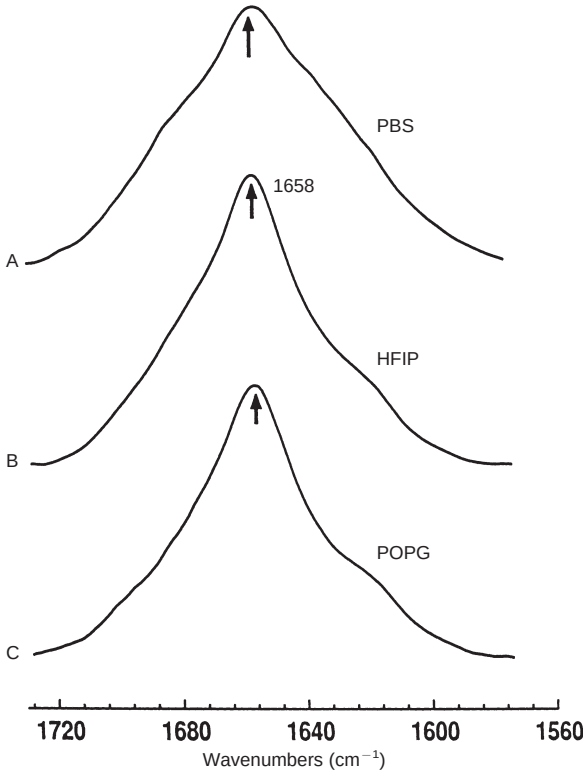

Figure 2. FTIR spectra of the amide I band of SP-B_{1-25} in PBS, HFIP solution and POPG liposomes. (A) The SP-B_{1-25} concentration was 341 μM in PBS, pH 7.4. (B) The SP-B_{1-25} concentration was 341 μM in HFIP/H_2O (7:3, v/v) with 10 mM phosphate, pH 7.4. (C) SP-B_{1-25} was added to POPG liposomes at an initial P/L of 1:70, suspended in PBS, pH 7.4. Peptide/liposomes were chromatographed to remove nonlipid-associated peptide, as described in Experimental procedures. Spectra were recorded at 25°C on chromatographed peptide/liposomes that were dried on the ATR and hydrated with D_2O for 2 h. The arrows indicate the α-helical band at 1658 cm^{-1}. Spectra were recorded at 25°C, and were normalized for comparison. The abscissa for each spectrum (left to right) is 1720–1580 cm^{-1}, while the ordinate represents absorption (in arbitrary units).

formalism of Chen *et al.* (43). This approach assumes that the maximum theoretical ellipticity for a given peptide or protein at 222 nm may be derived from the number of amino acid residues (n) and the ellipticity at 222 nm of a helix of infinite length described by equation 1:

$$\% \ \alpha\text{-helix} = [\Theta]_{MRE222}/[-39\,500\,(1 - (2.57/n))] \text{ deg cm}^2/\text{dmol} \quad (1)$$

FTIR Spectroscopy

Infrared spectra were recorded at 25°C using a Mattson Series FTIR spectrometer with a DTGS detector, averaged over 256 scans at a gain of 4 and a resolution of 2 cm^{-1} (33, 44). No nonlinear baseline corrections, water vapor subtractions, deconvolutions (except for the Fourier self-deconvolutions as noted below in Fig. 3) or smoothing operations were performed on the original spectra. For FTIR spectra of SP-B_{1-25} originally in solvents, peptide self-films were prepared by air drying peptide solutions [in 100% HFIP or aqueous 10 mM phosphate (pH 7.4)] onto 50 × 20 × 2 mm 45° ATR crystal (Spectral Solutions). For measurements with peptides in a lipid environment, SP-B_{1-25} peptides were added to LUV of POPG from the HFIP solution, and allowed to incubate with the liposomes for 1 h. FTIR spectra were measured on the above unchromatographed peptide/liposome mixtures, and also on these peptide/lipid samples after passing through a Sephadex G-50 column to remove nonliposome-associated peptide (45).

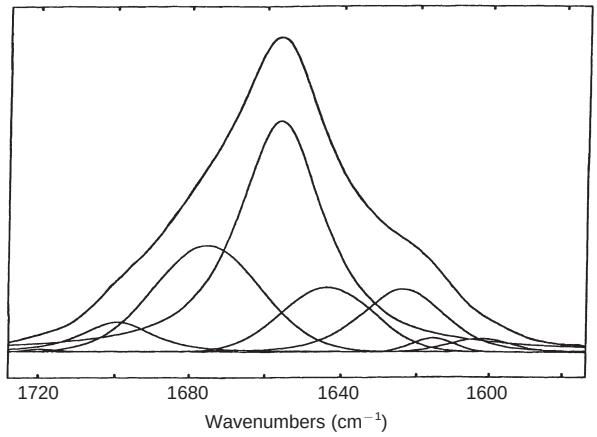

Figure 3. Representative FTIR spectrum and curve fitting of the amide I band of SP-B_{1-25} in POPG liposomes. (Top) The experimental FTIR spectrum of the amide I band (Fig. 2C). Frequency limits for different secondary structures were as follows: α-helix, 1662–1645 cm^{-1}; β-sheet, 1637–1613 cm^{-1} and 1689–1682 cm^{-1}; β-turn, 1682–1662 cm^{-1}; and disordered structure (random), 1650–1637 cm^{-1}. The percentage contributions for each component are shown in Table 3. Overlapping the experimental spectrum is the predicted spectrum, summing the above components. The initial peptide/lipid ratio was 1:70, for SP-B_{1-25} added to POPG liposomes. Peptide/liposomes were chromatographed to remove nonlipid-associated peptide, as described in Experimental procedures.

Chromatographed and unchromatographed lipid–peptide samples were dried onto the ATR crystal. Both peptide–self-film and lipid–peptide samples were then hydrated for 2 h by passing nitrogen–D_2O vapor through ports in the cell body. Martin *et al*. (45) noted earlier that the peptide concentration is proportional to the area (S_{amide}) of the amide I band (1680–1600 cm^{-1}), while the lipid concentration is proportional to the area ($S_{\nu\ (C=O)lipid}$) of the lipid ν (C=O) band (1770–1700 cm^{-1}). Accordingly, the peptide/lipid ratio is proportional to the following: (S_{amide})/($S_{\nu\ (C=O)lipid}$).

The amide I bands of conventional ^{12}C-FTIR spectra of peptide self-films and chromatographed lipid/peptide samples were analyzed for the various SP-B_{1-25} conformations (33). For determinations with peptide/liposomes, the spectrum of the lipid film without peptide (i.e. the band centered at 1730 cm^{-1}) was subtracted from that of samples with peptide associated with lipid. The amounts of α-helix, β-turn, β-sheet and disordered conformations were determined by Fourier self-deconvolutions for band narrowing and area calculations of component peaks determined using curve fitting software supplied by Mattson and based on procedures described by Kauppine *et al*. [46]. The frequency limits for the different structures were as follows: α-helix (1662–1645 cm^{-1}), β-sheet (1637–1613 cm^{-1} and 1689–1682 cm^{-1}), β-turns (1682–1662 cm^{-1}) and disordered or random (1650–1637 cm^{-1}) (47–49).

Enhancement of SP-B_{1-25} peptides with site-specific ^{13}C-carbonyl groups permits the direct determination of those amino acid residues participating in secondary conformations. Since the stretching frequencies of the peptide backbone carbonyl groups are sensitive to local conformations, replacement of ^{12}C with ^{13}C should reduce the stretching frequency of an isolated carbonyl oscillator by ≈ 37 cm^{-1} (35, 50, 51). Specifically, the α-helix band should be lowered to 1625–1608 cm^{-1}, the β-sheet to 1600–1576 cm^{-1} and 1652–1645 cm^{-1}, β-turns to 1645–1625 cm^{-1} and disordered or random to 1613–1600 cm^{-1}. These spectral shifts were detected by measuring FTIR spectra of the natural abundance and ^{13}C-enhanced peptides in various environments (35, 36); subtle spectral shifts were also detected with difference FTIR spectra, obtained by subtracting the natural abundance spectrum from that of the isotopically enhanced peptide (35). The difference FTIR spectra should show a negative peak at the original position of the conformational band, and a positive peak shifted from the original by ≈ 37 cm^{-1}. Unless distorted by noise, the negative peak for a given conformational band should be symmetrical to the positive peak about an inflection point.

Molecular modeling

The N-terminal peptide of human SP-B, SP-B_{1-25}, was modeled using Insight/Discover 97.0 software (Molecular Simulations, San Diego, CA, USA) running on a Silicon Graphics Indigo-2R10000 High Impact workstation (Beckman Research Institute City of Hope Core Facility). Energy minimizations and molecular dynamics were conducted using the CVFF force field (52, 53) within the Discover software environment. Ramachandran plots were determined for the SP-B_{1-25} structures derived from simulated annealing. The final refined model geometry parameters were evaluated by PROCHECK (54).

Coordinates

The coordinates for the 10 lowest energy structures of SP-B_{1-25} in POPG, together with a full list of restraints, have been deposited in the Protein Data Bank under the accession code 1DFW.

Results

CD Spectroscopy

To assess the overall conformation of the N-terminal sequence of SP-B ($SP\text{-}B_{1-25}$) in a variety of environments, CD spectra were recorded for peptide in an aqueous buffer, a membrane-mimic solvent or a liposome suspension. For example, Fig. 1A shows representative CD spectra of $SP\text{-}B_{1-25}$ suspended in either an aqueous environment (i.e. PBS, pH 7.4) or a membrane-mimetic solvent (i.e. HFIP/H_2O with 10 mM phosphate, pH 7.4). The PBS and HFIP spectra in Fig. 1A each demonstrate a characteristic double minimum at 208 and 222 nm, suggesting a considerable α-helical content for $SP\text{-}B_{1-25}$. The corresponding CD spectrum (Fig. 1B) of $SP\text{-}B_{1-25}$ with POPG liposomes in PBS, pH 7.4, after chromatography to remove unbound peptide, similarly indicates a broad double minimum at 208 and 222 nm that is characteristic of high α-helix.

It is worthwhile quantitating the $SP\text{-}B_{1-25}$ conformation with further analysis of the CD spectra (Fig. 1). The percentage of α-helix conformation for the peptide was estimated according to equation 1, as described above (43). Similar elevated proportions of α-helix (i.e. 50–66%) were determined for $SP\text{-}B_{1-25}$ in the respective PBS, HFIP and POPG environments (Table 3). The relatively high noise for the PBS spectrum in Fig. 1A was attributed to both the limited solubility of amphipathic peptide in aqueous medium and increased light scattering due to the formation of $SP\text{-}B_{1-25}$ microaggregates. Previous ESR studies (33) of spin-labeled $SP\text{-}B_{1-25}$ in PBS indicated low solubility and elevated aggregation at high peptide concentrations (≥ 109 μM), similar to those used here in CD measurements (Fig. 1A). The elevated noise in the POPG spectrum (Fig. 1B) might be a consequence of enhanced light scattering due to $SP\text{-}B_{1-25}$-promoted liposome aggregation (27).

Conventional ^{12}C-FTIR spectroscopy

The secondary conformations of $SP\text{-}B_{1-25}$ in the above solvent and lipid systems were then investigated using conventional ^{12}C-FTIR spectroscopy. Typical FTIR spectra of the amide I band are shown in Fig. 2, and were similar for the three environments. A dominant band occurs at 1658 cm^{-1} for the PBS (Fig. 2A), HFIP (Fig. 2B) and POPG (Fig. 2C) systems, indicative of high α-helical content for $SP\text{-}B_{1-25}$. Subsequent curve fitting of the POPG spectrum using the criteria of Byler & Susi (47) confirmed a high proportion of $SP\text{-}B_{1-25}$ as α-helix, with much smaller contributions due to β-sheet, β-turn and disordered or random structure (Fig. 3; Table 3). For the 25 amino acid sequence $SP\text{-}B_{1-25}$ in POPG, the FTIR analysis in Table 3 suggests that this peptide has ≈ 13 residues as α-helix, ≈ 9 residues as β-conformations and ≈ 3 residues as random structure. Deconvolution of the FTIR spectra of $SP\text{-}B_{1-25}$ in either the PBS or the HFIP solvent systems indicated comparable proportions of secondary structure (Table 3).

The association of $SP\text{-}B_{1-25}$ with POPG liposomes was quantified by recording ^{12}C-FTIR spectra, before (not shown) and after chromatographing peptide/lipid mixtures. For POPG incubated with $SP\text{-}B_{1-25}$ at an initial calculated peptide/lipid (P/L) ratio of 1:70, the $(S_{amide})/(S_{\nu(C=O)lipid})$ ratio for unchromatographed and chromatographed samples indicated > 80% peptide uptake by liposomes. These results are consistent with the relatively low solubility of the peptide in PBS buffer, and the probable strong association between this cationic, amphipathic $SP\text{-}B_{1-25}$ and the anionic, polar headgroup region of POPG (see below) (33).

Isotopically enhanced ^{13}C-FTIR spectroscopy of cassette-labeled $SP\text{-}B_{1-25}$ in POPG liposomes

Although the above ^{12}C-FTIR spectroscopic findings indicate that $SP\text{-}B_{1-25}$ is conformationally heterogeneous when bound to POPG liposomes (Fig. 3; Table 3), it is not possible using only this data to assign the secondary conformations (i.e. α-helix, β-turn, β-sheet, random) to specific residues. To probe local conformations within the peptide, isotopically enhanced, FTIR spectroscopy was performed with $SP\text{-}B_{1-25}$ labeled with ^{13}C-carbonyl groups at multiple sites (Table 1). For peptides incorporated into POPG liposomes, Fig. 4 shows the natural abundance, ^{12}C-FTIR spectrum of $SP\text{-}B_{1-25}$ and the isotopically enhanced, ^{13}C-FTIR spectra of a suite of cassette-labeled $SP\text{-}B_{1-25}$. There are major differences between the native and cassette-labeled $SP\text{-}B_{1-25}$ spectra, which are attributed to the presence of ^{13}C-carbonyl groups.

The putative β-conformation for the N-terminal region of $SP\text{-}B_{1-25}$, predicted theoretically (13, 30) and experimentally using truncated peptides (33), was tested here by comparing the FTIR spectra of native $SP\text{-}B_{1-25}$ with that of $SP\text{-}B_{1-25}$ (F1/L3/I5) (Table 1). In the $SP\text{-}B_{1-25}$ (F1/L3/I5) spectrum (Fig. 4A), there is a large decrease in the area 1637–1613 cm^{-1} corresponding to β-sheet, and a concurrent increase in the area 1600–1576 cm^{-1}, indicating an isotopic shift of ≈37 cm^{-1}. The nature of this isotopic shift is visualized more readily in a difference FTIR spectrum, obtained by subtracting the native FTIR spectrum (dashed line in Fig. 4A) from that of the $SP\text{-}B_{1-25}$ (F1/L3/I5) spectrum (solid line in Fig. 4A); the

Table 3. **Proportions of secondary structure[a] for SP-B_{1-25} in solvents and POPG lipid dispersions, as estimated from Fourier self-deconvolution of the FTIR spectra of the peptide amide I band and CD spectra**

System	% Conformation α-Helix	β-Sheet	β-Turn	Disordered
FTIR Spectra[b]				
PBS[c]	50	10	32	8
HFIP[d]	54	7	25	14
POPG[e]	52	12	24	12
CD Spectra[f]				
PBS[g]	50	ND[j]	ND	ND
HFIP[h]	66	ND	ND	ND
POPG[i]	53	ND	ND	ND

a. Data are the means of four separate determinations and have an SE ± 5% or better. b. FTIR spectra were deconvoluted as described in Experimental procedures (Fig. 3). c. SP-B_{1-25} (341 μM) dried on to the ATR from PBS, pH 7.4. (Fig. 2A). d. SP-B_{1-25} (341 μM) dried on to an ATR plate from hexafluoroisopropanol (HFIP)/water (7:3, v/v) in 10 mM phosphate, pH 7.4. (Fig. 2B). e. Chromatographed SP-B_{1-25}:POPG liposomes (initial peptide/lipid (P/L) ratio, 1:70) in PBS, pH 7.4, dried on to an ATR plate. (Fig. 2C). f. CD spectra were analyzed with the method of Chen *et al*. (43) (Fig. 1). g. SP-B_{1-25} suspended in phosphate buffered saline, pH 7.4 at 225 μM (Fig. 1A). h. SP-B_{1-25} in HFIP/water (7:3, v/v) with 10 mM phosphate, pH 7.4 at 173 μM (Fig. 1A). i. Chromatographed SP-B_{1-25}:POPG (initial P/L, 1:70) in PBS, pH 7.4. (Fig. 1B). j. ND, not determined.

resulting difference FTIR spectrum (Fig. 5A) confirms the presence of negative and positive bands centered at 1623 cm^{-1} and 1588 cm^{-1}, respectively. The simplest interpretation of these results is that, in the native SP-B_{1-25} spectrum, residues Phe^{1}, Leu^{3} and Ile^{5} contribute to the β-sheet band identified in the Fourier deconvoluted spectrum at 1637–1613 cm^{-1} (Figs 3 and 6).

The proposed α-helical conformation for the C-terminal region of SP-B_{1-25}, predicted theoretically (6) and experimentally using truncated peptides (33, 34), was similarly investigated here with cassette ^{13}C-labeled SP-B_{1-25} peptides (Table 1). The local conformations for residues 8 and 11 of SP-B_{1-25} were determined by comparing the ^{13}C-enhanced SP-B_{1-25} (A8/A11) spectrum with that of the native peptide. For the SP-B_{1-25} (A8/A11) spectrum in Fig. 4B, the band at 1662–1645 cm^{-1} corresponding to α-helix is reduced with a new band concurrently arising at 1625–1608 cm^{-1}, indicating an isotopic shift of 37 cm^{-1}. The difference FTIR spectrum for SP-B_{1-25} (A8/A11) in Fig. 5B, obtained by subtracting the native spectrum (dashed line in Fig. 4B) from that of SP-B_{1-25} (A8/A11) (solid line in Fig. 4B), confirms the presence of negative and positive bands centered at 1658 and 1621 cm^{-1}, respectively. Since substitution of Ala for Cys residues does not affect the conformation of SP-B_{1-25} bound to lipids (24), these FTIR spectral findings for SP-B_{1-25} (A8/A11) suggest that Cys^{8} and Cys^{11} each contribute to the α-helix band identified in the Fourier deconvoluted spectrum at 1662–1645 cm^{-1} (Figs 3 and 6). It is of particular interest that the FTIR spectrum of SP-B_{1-25} (L10/A13/L14) (Fig. 4C), and also the difference FTIR spectrum (Fig. 5C), obtained by subtracting the native SP-B_{1-25} spectrum (Fig. 4C; dashed line) from that of SP-B_{1-25} (L10/A13/L14), are nearly identical to those obtained for SP-B_{1-25} (A8/A11) (Figs 4B and 5B). Because the SP-B_{1-25} (A8/A11) and SP-B_{1-25} (L10/A13/L14) have overlapping ^{13}C-enhanced amino acids, these results indicate that the α-helix extends from Cys^{8} until at least Leu^{14} (Fig. 6).

The corresponding FTIR spectral results of another cassette, SP-B_{1-25} (I18/A20/I22), provide some evidence that the α-helix terminates at Ile^{22}. For the SP-B_{1-25} (I18/A20/I22) spectrum in Fig. 4D, the band at 1662–1645 cm^{-1} is reduced with respect to the native spectrum, with a new band arising concurrently at 1620–1603 cm^{-1}, indicating an isotopic shift of 42 cm^{-1}. The difference FTIR spectrum for SP-B_{1-25} (I18/A20/I22) in Fig. 5D confirms the presence of negative and positive bands centered at 1658 and 1615 cm^{-1}, respectively. One possible interpretation is that only one of the ^{13}C-carbonyls of SP-B_{1-25} (I18/A20/I22) participates in the α-helix; this would be consistent with the relatively modest decrease in the α-helical band at 1662–1645 cm^{-1} and the much larger isotopic shift for the new peak (Fig. 4D) than those of SP-B_{1-25} (L10/A13/L14) (Fig. 4C). Here, the positive band centered at 1615 cm^{-1} (Figs 4D and 5D) would itself be a composite, because of the ^{13}C-carbonyls of Ile^{18}, Ala^{20} and Ile^{22} of SP-B_{1-25} (I18/A20/I22) assuming α-helical and other conformations. In this context, it is important to note that the helix-breaking Pro^{23} prevents the carbonyl of Ala^{20} hydrogen bonding to Lys^{24} as an α-helix. Accordingly, the ^{13}C-carbonyl of Ile^{18} may participate in the α-helix by bonding to the amide hydrogen of Ile^{22}, whereas the corresponding carbonyls of Ala^{20} and Ile^{22} assume other conformations (Fig. 6). The only α-helical involvement for the Ala^{20} and Ile^{22} residues would be through donation of amide hydrogens to their respective carbonyl partners, Lys^{16} and Ile^{18} (see below).

Isotopically enhanced ^{13}C-FTIR spectroscopy of single residue-labeled SP-B_{1-25} in POPG liposomes

The local conformations within the peptide were also probed using FTIR spectroscopy of SP-B_{1-25} labeled with ^{13}C-carbonyl groups at single sites (Table 2). The use of such labeled peptides allows study of whether a given residue is flexible enough to exhibit multiple conformations. Single-site ^{13}C-carbonyl-labeled peptides are particularly advantageous in assessing α-helical domains. For a residue (N)

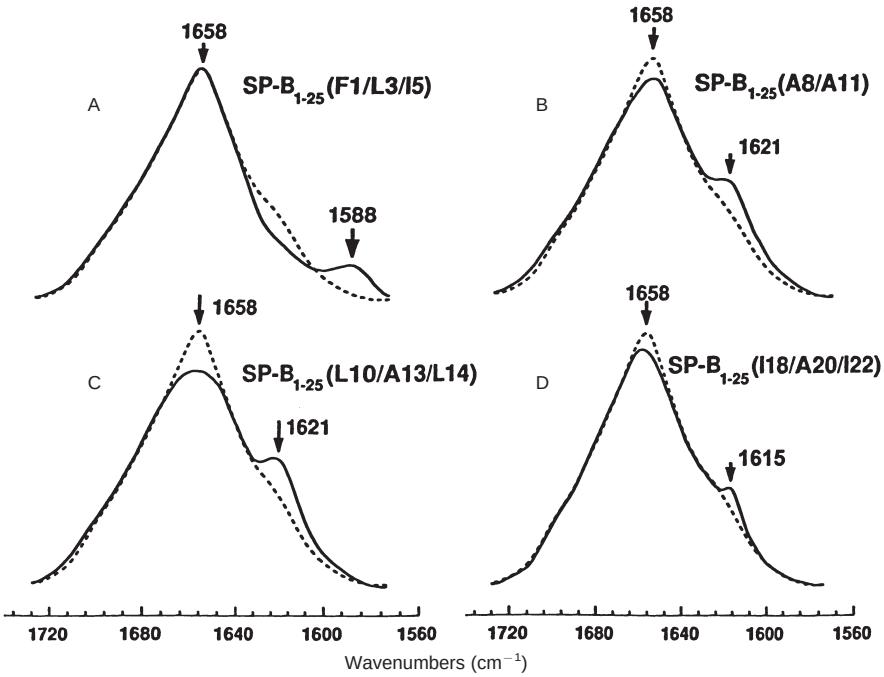

Figure 4. FTIR spectra of the amide I band for the ^{12}C-carbonyl (i.e. native) SP-B_{1-25} peptide and a suite of multiply ^{13}C-carbonyl enhanced (i.e. cassette)-labeled SP-B_{1-25} peptides in POPG liposomes. Peptides at an initial P/L ratio of 1:70 were added to POPG liposomes suspended in PBS, pH 7.4. Spectra were recorded at 25°C on chromatographed peptide/liposomes that were dried on the ATR and hydrated with D_2O for 2 h. (A) SP-B_{1-25} (F1/L3/I5) is the solid line and native SP-B_{1-25} is the dashed line. The amide I band is shown for the native SP-B_{1-25} spectrum, with a dominant α-helical component centered at 1658 cm^{-1}. The peak at 1588 cm^{-1} in the SP-B_{1-25} (F1/L3/I5) spectrum indicates β-sheet for Phe^{1}, Leu^{3} and Ile^{5}. (B) SP-B_{1-25} (A8/A11) (solid line), SP-B_{1-25} (dashed line). The peak at 1621 cm^{-1} in the SP-B_{1-25} (A8/A11) spectrum indicates α-helix for Ala^{8} and Ala^{11}. (C) SP-B_{1-25} (L10/A13/L14) (solid line), SP-B_{1-25} (dashed line). The peak at 1621 cm^{-1} in the SP-B_{1-25} (L10/A13/L14) spectrum indicates an α-helix for Leu^{10}, Ala^{13} and Leu^{14}. (D) SP-B_{1-25} (I18/A20/I22) (solid line), SP-B_{1-25} (dashed line). The peak at 1615 cm^{-1} in the SP-B_{1-25} (I18/A20/I22) spectrum indicates an α-helical contribution for Ile^{18}, Ala^{20} and Ile^{20}. See Table 1 for amino acid sequences for SP-B_{1-25} and ^{13}C-enhanced SP-B_{1-25} peptides. Spectra and peak assignments are representative of three independent experiments.

whose carbonyl group forms an α-helical C=O····H–N hydrogen bonding with its residue partner (N + 4), the FTIR assignment of an α-helix to the ^{13}C-carbonyl N-residue also confirms α-helical conformations for four consecutive residues: N + 1, N + 2, N + 3 and N + 4 (36).

The conformation of the C-terminus of SP-B_{1-25} bound to POPG liposomes was studied by comparing the FTIR spectrum of native SP-B_{1-25} with that of SP-B_{1-25} (G25; Table 2). In the SP-B_{1-25} (G25) spectrum (Fig. 7C), there is a small decrease in the area (1650–1637 cm^{-1}) corresponding to random structure, as well as an increase in the area 1613–1600 cm^{-1}, indicating an isotopic shift of ≈ 37 cm^{-1}. This isotopic shift is seen more clearly in the corresponding difference FTIR spectrum (Fig. 7D), which confirms negative and positive bands centered at 1647 cm^{-1} and 1606 cm^{-1}, respectively. The results suggest that, in the native SP-B_{1-25} spectrum, residue Gly^{25} contributes to the random structural band identified in the Fourier deconvoluted spectrum at 1650–1637 cm^{-1} (Figs 3 and 6).

The α-helical structure for SP-B_{1-25}, tentatively assigned in Fig. 6 from FTIR spectroscopy of cassette ^{13}C-labeled peptides, was examined further using single-site ^{13}C-carbonyl-labeled SP-B_{1-25} peptides (Table 2). Residue 8 of SP-B_{1-25} was investigated by recording the FTIR spectrum of SP-B_{1-25} (A8) incorporated into POPG liposomes. Both the FTIR spectrum (Fig. 8A) and the difference FTIR spectrum (Fig. 8B) of SP-B_{1-25} (A8) show that the major conformation at position 8 (Cys^{8} in native peptide) is α-helical, as indicated by the additional positive band at 1618 cm^{-1}; the small, second positive band at 1637 cm^{-1} in the difference FTIR spectrum (Fig. 8B) also reflects a minor β-turn element for position 8. Apparently, position 8 for SP-B_{1-25} is conformationally flexible, assuming primarily an α-helical conformation with a minor β-turn element (Fig. 6). These experiments were repeated with additional single-site ^{13}C-carbonyl-enhanced SP-B_{1-25} peptides to determine the conformation of positions 11, 15 and 18 (Table 2). The respective FTIR spectra and difference FTIR spectra for

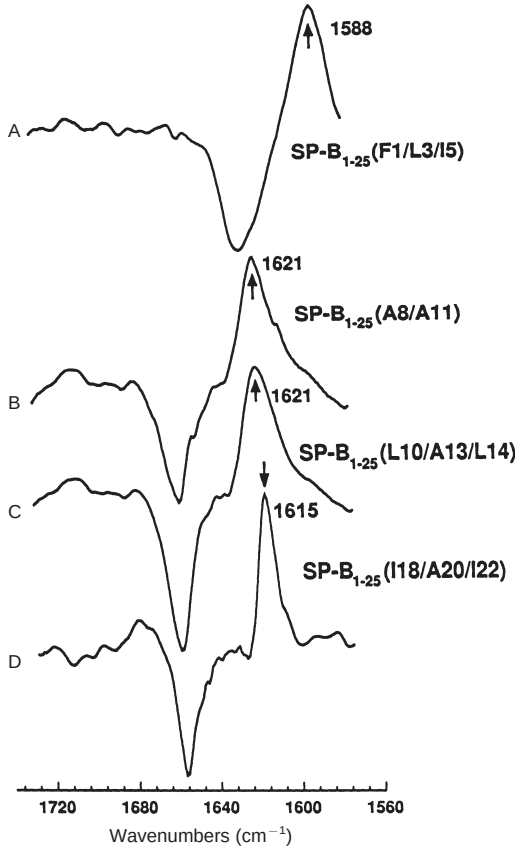

Figure 5. Difference FTIR spectra of SP-B_{1-25} peptides with POPG liposomes in PBS, pH 7.4, obtained by subtracting the spectrum of the native ^{12}C-carbonyl SP-B_{1-25} from those of multiply ^{13}C-carbonyl-enhanced SP-B_{1-25} peptides. (A) SP-B_{1-25} spectrum (dashed line in Fig. 4A) from SP-B_{1-25} (F1/L3/I5) spectrum (solid line in Fig. 4A). The peak at 1588 cm^{-1} (arrow) indicates a β-sheet for Phe^{1}, Leu^{3} and Ile^{5}. (B) SP-B_{1-25} spectrum (dashed line in Fig. 4B) from SP-B_{1-25} (A8/A11) (solid line in Fig. 4B). The peak at 1621 cm^{-1} (arrow) indicates an α-helix for Ala^{8} and Ala^{11}. (C) SP-B_{1-25} spectrum (dashed line in Fig. 4C) from SP-B_{1-25} (L10/A13/L14) (solid line in Fig. 4C). The peak at 1621 cm^{-1} (arrow) indicates an α-helix for Leu^{10}, Ala^{13} and Leu^{14}. (D) SP-B_{1-25} spectrum (dashed line in Fig. 4D) from SP-B_{1-25} (I18/A20/I22) (solid line in Fig. 4D). The peak at 1615 cm^{-1} indicates an α-helical contribution for Ile^{18}, Ala^{20} and Ile^{22}. See Table 1 for amino acid sequences of the native and ^{13}C-enhanced SP-B_{1-25} peptides. The abscissa for each spectrum (left to right) is 1720–1580 cm^{-1}, while the ordinate represents Δ (absorption), in arbitrary units. The peak-to-trough amplitudes for each spectrum were normalized. Spectra and peak assignments are representative of three independent experiments.

SP-B_{1-25} (A11) (Fig. 8C, D), SP-B_{1-25} (I15) (Fig. 7A, B) and SP-B_{1-25} (I18) (Fig. 9A, B) all show positive bands at 1618–1620 cm^{-1}, consistent with α-helical conformations for positions 11, 15 and 18 (Fig. 6). Following the above argument of Ludlam *et al.* (36), our finding of primarily α-helical participation for the carbonyls of residues 8, 11, 15 and 18 further requires that the entire peptide segment Cys^{8} to Ile^{22} is α-helical. It is of particular interest to note that the difference FTIR spectrum for SP-B_{1-25} (I18) indicates an α-helical conformation for Ile^{18} (i.e. a positive peak at 1618 cm^{-1} in Fig. 9B), while the corresponding difference FTIR spectrum for SP-B_{1-25} (A20) reports β-turn and random conformations for Ala^{20} (i.e. peaks at 1627 and 1608 cm^{-1} in Fig. 9D). These results confirm our preliminary assignment that the FTIR spectrum of SP-B_{1-25} (I18/A20/I22) is a composite, arising from the carbonyl of Ile^{18} participating in an α-helix (through bonding with the amide H of Ile^{22}) with the carbonyls of Ala^{20} and Ile^{22} assuming other conformations. The finding of multiple conformations for the carbonyl groups at the ends of the α-helix for SP-B_{1-25} (Fig. 6) suggests some fraying of the helix at the N- and C-termini.

Molecular modeling

Although the above ^{13}C-FTIR spectroscopic analysis assigned the conformation of the majority (> 75%) of the amino acids for SP-B_{1-25} in POPG liposomes, the conformations of a number of residues (i.e. Pro^{2}, Pro^{4}, Pro^{6}, Tyr^{7}, Pro^{23}, Lys^{24}) were not determined experimentally. Molecular modeling was conducted to provide structural information on these 'gap' residues, and also to assess the conformational flexibility of domains within SP-B_{1-25}. From the ^{13}C-FTIR spectral results in Fig. 6, the initial structure was modeled as an α-helix, except for the terminal regions (residues 1–7 and 22–25), which were modeled as β-strands using Discover software. Ten cycles of simulated annealing were performed, using a protocol published earlier (55), to explore those conformations accessible to the terminal regions and helix side-chains. Throughout the simulation, constraints were applied to the helix backbone so that the structure would remain consistent with data derived from ^{13}C-FTIR spectroscopic mapping studies. Using a time step of 0.5 fs, the system was equilibrated for 1000 iterations at 300 K. The temperature was then increased to 900 K in increments of 30 K over a period of 20 ps. Molecular dynamics was then carried out at 900 K for 30 ps, followed by annealing to a temperature of 300 K over 50 ps. The resulting structure was then energy minimized (52, 53) using 5000 steps, followed by 10 000 steps of conjugate gradients until the maximum derivative was < 0.001. Throughout the simulation, the backbone atoms of residues 8–22 were constrained using a force constant that increased by 100 [kCal/mol × Å^{2}] during each heating step. A similar torsional constraint was applied to all peptide bonds to maintain them in the *trans* conformation.

With the residue-specific constraints based on ^{13}C-FTIR measurements described above, 10 molecular models

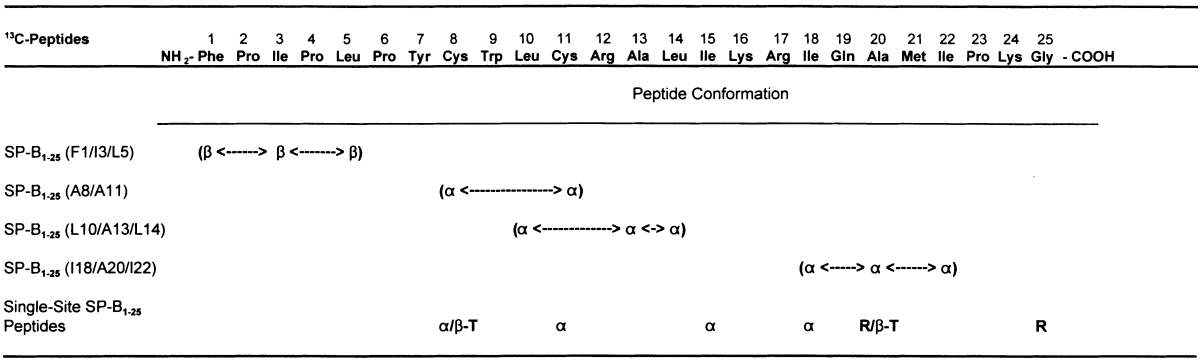

Figure 6. Conformational map of the N-terminal peptide of SP-B ($SP\text{-}B_{1-25}$) in the lipid POPG, as estimated from the FTIR spectra of ^{13}C-labeled peptides. Amino acids are represented by three-letter codes. Peptides, at a P/L ratio of 1:70, were added to POPG liposomes suspended in PBS. Codes (in parentheses) for peptide conformations are: β-sheet (β), β-turn (β-T), α-helix (α) and random (R). Secondary conformations were determined for $SP\text{-}B_{1-25}$ peptides labeled with ^{13}C at multiple sites (Table 1) by recording the FTIR spectra of $SP\text{-}B_{1-25}$ (F1/I3/L5) in Fig. 4A, $SP\text{-}B_{1-25}$ (A8/A11) in Fig. 4B, $SP\text{-}B_{1-25}$ (L10/A13/L14) in Fig. 4C and $SP\text{-}B_{1-25}$ (I18/A20/I22) in Fig. 4D. Secondary conformations were also determined for $SP\text{-}B_{1-25}$ labeled with ^{13}C at single sites (Table 2) by recording the FTIR spectra shown in Figs 7–9.

representing possible lipid conformations of $SP\text{-}B_{1-25}$ were generated by simulated annealing molecular dynamics. The superimposed conformers are shown as stick figure representations in Fig. 10A, whereas a ribbon representation of a selected conformer showing the location of each residue is indicated in Fig. 10B. The geometry parameters of the final conformer models were evaluated using PROCHECK (54). The Ramachandran plot in Fig. 11 verifies that the backbone torsion angles for all 10 conformers fell within the allowed regions. Furthermore, the Ramachandran plot indicates high levels of backbone torsion angles lying in the α-helix and β-structural zones, consistent with the structure of $SP\text{-}B_{1-25}$ principally subdivided into α-helix and β-conformations (Fig. 11). The superimposed conformers capture the major structural features indicated by our ^{13}C-FTIR spectra, namely an α-helix (residues 8–22) capped with Pro^{6} and Pro^{23}, a β-conformation at the N-terminal sequence (residues 1–6) and random structure at the C-terminus (residues 23–25). Within the helix, several alternative packing arrangements are accessible to the side-chains. It is interesting to note that, in the modeled structures of Fig. 10A, the side-chain of Tyr^{7} often packs against the side-chains of the $i + 3$ residue (Leu^{10}), an interaction that is believed to be helix stabilizing (56). In our models, Tyr^{7} is the residue that appears to initiate the helix, its carbonyl group being the first to participate in the helix hydrogen-bonding network. The β-conformation structure for the N-terminal sequence (residues 1–6) exhibits considerable flexibility in Fig. 10A, evincing some ability to fold on itself as an antiparallel β-sheet. Since the α-helix was constrained as an initial condition throughout, one important limitation of this modeling exercise is that it is unable to demonstrate any fraying at the two ends of the α-helix. The pleiomorphism that was noted at the ends of the α-helix in Fig. 6 may be due to the lack of hydrogen bonding that occurs at N- and C-terminal caps.

Discussion

The residue-specific conformational model for $SP\text{-}B_{1-25}$ in lipid (Figs 6 and 10), developed here using ^{13}C-FTIR spectroscopy and molecular modeling, is broadly in agreement with previous theoretical predictions and physical measurements on the full-length (25 residue) peptide. Consistent with earlier Chou–Fasman predictions of secondary structure (30, 32), β-conformations were concentrated in the N-terminal region with an α-helix in the C-terminal domain (Figs 6 and 10). It is also important to compare the α-helical content reported here from CD spectroscopy of $SP\text{-}B_{1-25}$ in POPG liposomes (Fig. 1B; Table 3) with that obtained from ^{13}C-FTIR spectroscopy (Figs 6 and 10B). Both CD and site-directed ^{13}C-FTIR spectroscopic analyses indicate similar α-helical content (i.e. 53 and 60%, respectively) for $SP\text{-}B_{1-25}$ in POPG liposomes. These results are of particular interest, given that CD spectroscopy used continuously hydrated peptide/liposomes, whereas ATR-FTIR spectroscopy subjected samples to a drying and rehydration step. Our finding of similar total α-helical content from these two techniques argues against the drying and rehydration step introducing significant experimental artifacts into the ^{13}C-FTIR spectral analysis. In agreement with this are our observations that dried and rehydrated FTIR samples possess relatively high levels of hydration. Okamura *et al.* (57) previously showed that the hydration state of DPPC multilayers could be determined using FTIR spectroscopy, by noting that the

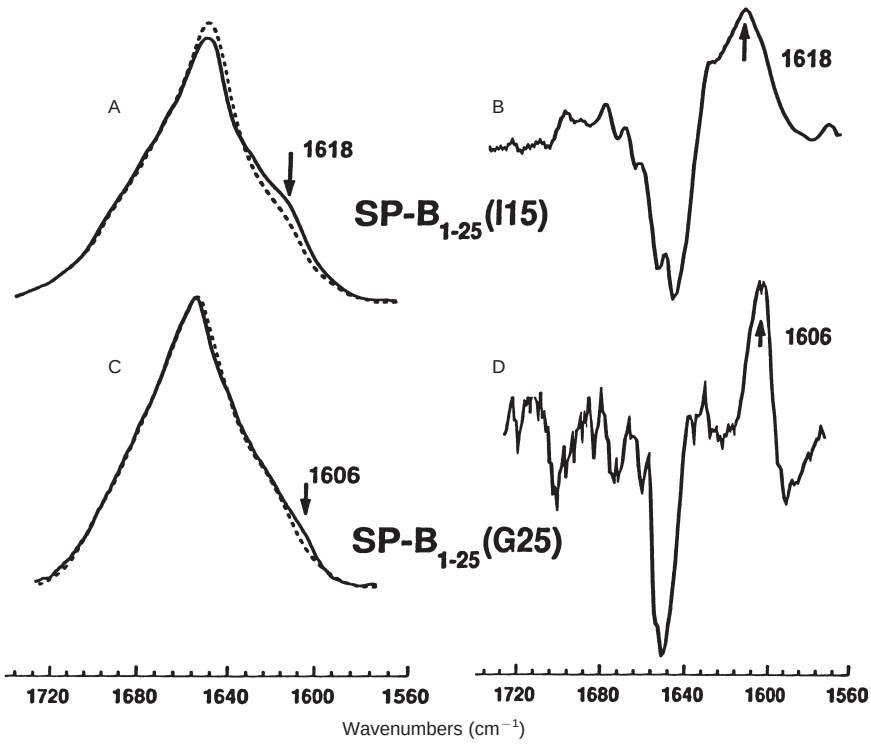

Figure 7. FTIR and difference FTIR spectra of the amide I band for ^{12}C-carbonyl SP-B_{1-25} (native) and single ^{13}C-carbonyl-enhanced SP-B_{1-25} peptides labeled at Ile^{15} [i.e. SP-B_{1-25} (I15)] or Gly^{25} [i.e. SP-B_{1-25} (G25)]. Peptides at an initial P/L ratio of 1:70 were added to POPG liposomes suspended in PBS, pH 7.4. Spectra were recorded at 25°C on chromatographed peptide/liposomes that were dried on the ATR and hydrated with D_2O for 2 h. (A) SP-B_{1-25} (I15) is the solid line and native SP-B_{1-25} is the dashed line. The minor peak at 1618 cm^{-1} in the SP-B_{1-25} (I15) spectrum indicates an α-helix for Ile^{15}. (B) SP-B_{1-25} spectrum (dashed line in A) from SP-B_{1-25} (I15) (solid line in A). The peak at 1618 cm^{-1} (arrow) indicates an α-helix for Ile^{15}. (C) SP-B_{1-25} (G25) is the solid line and native SP-B_{1-25} is the dashed line. The minor peak at 1606 cm^{-1} in the SP-B_{1-25} (G25) spectrum indicates a random conformation for Gly^{25}. (D) SP-B_{1-25} spectrum (dashed line in C) from SP-B_{1-25} (G15) (solid line in C). The peak at 1606 cm^{-1} (arrow) indicates a random conformation for Gly^{25}. See Table 2 for amino acid sequences of peptides. Spectra and peak assignments are representative of three independent experiments.

intensity ratio of the OH stretching band of water (at 3380 cm^{-1}) to the CH_2 band of lipid (at 2928 cm^{-1}) is proportional to the hydration state (% weight). Following this approach, our FTIR samples rehydrated for 2 h indicated substantial D_2O content, with an intensity ratio of 2.5 for the OD stretching band of D_2O (at 2493 cm^{-1}) to that of the CH_2 band of lipid (at 2925 cm^{-1}) (spectra not shown). Also in support of our view that the drying and rehydration step does not introduce errors, Goormaghtigh *et al.* (58) reported no differences for FTIR spectra of selected proteins recorded either by transmission in solution or by drying and rehydration on the ATR crystal.

It is also important to note that the proportions of secondary conformation determined by Fourier self-deconvolution of ^{12}C-FTIR spectra of SP-B_{1-25} in POPG liposomes (i.e. ≈ 13 residues as α-helix, ≈ 9 residues as β-conformations and ≈ 3 residues as random structure; Fig. 3; Table 3) are in good agreement with those determined from site-directed ^{13}C-FTIR spectroscopy and modeling (≈ 15 residues as α-helix, ≈ 7 residues as β-conformations and ≈ 3 residues as random; Figs 6 and 10). Fourier self-deconvolution of FTIR spectra is a standard technique used to estimate the proportions of secondary structure in peptides and proteins (47, 49). With this computer-fitting methodology, the integrated intensities of the component band are proportional to the populations of the conformational structures represented by these components. The relative percentages of secondary structures may be determined by adding the areas of all bands assigned to each of these structural elements, and then expressing the sum as a fraction of the total amide I band area (48). Since Fourier self-deconvolution assumes that the intrinsic absorption of each structural component will be similar in all peptides and proteins, Surewicz & Mantsch (48) believed that the percent conformations derived with this approach should be viewed as estimates only. Despite these uncertainties, however, good correlations were reported for a wide range of proteins between the secondary structures determined from X-ray diffraction and Fourier self-deconvolution of FTIR spectra (47, 49). Here, the percent secondary structures were assessed for SP-B_{1-25} in POPG liposomes using both Fourier self-deconvolution (Fig. 3; Table 3) and ^{13}C-FTIR spectroscopy (Figs 6 and 10B). Such comparisons are a further independent test of the Fourier self-deconvolution technique, because the experimental conditions for Fourier self-deconvolution and site-directed ^{13}C-FTIR spectroscopy are virtually identical (except for the use of ^{13}C-labeled peptides), and no assumptions are made in ^{13}C-FTIR

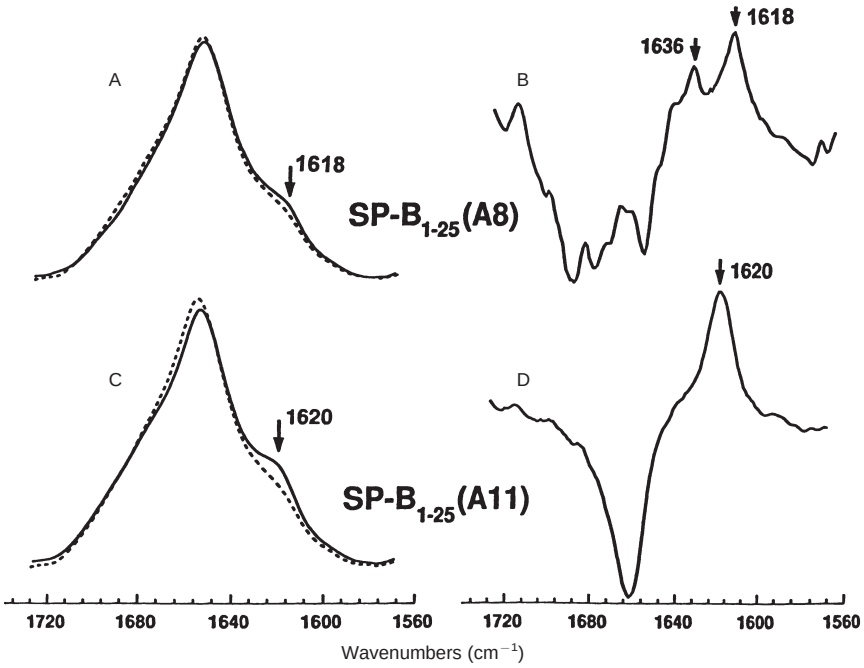

Figure 8. FTIR and difference FTIR spectra of the amide I band for ^{12}C-carbonyl SP-B_{1-25} (native) and single ^{13}C-carbonyl enhanced SP-B_{1-25} peptides labeled at Ala^{8} [i.e. SP-B_{1-25} (A8)] or Ala^{11} [i.e. SP-B_{1-25} (A11)]. Peptides at an initial P/L ratio of 1:70 were added to POPG liposomes suspended in PBS, pH 7.4. Spectra were recorded at 25°C on chromatographed peptide/liposomes that were dried on the ATR and hydrated with D_2O for 2 h. (A) SP-B_{1-25} (A8) is the solid line and native SP-B_{1-25} is the dashed line. The minor peak at 1618 cm^{-1} in the SP-B_{1-25} (A8) spectrum indicates an α-helix contribution for Ala^{8}. (B) SP-B_{1-25} spectrum (dashed line in A) from SP-B_{1-25} (A8) (solid line in A). The major peak at 1618 cm^{-1} and minor peak at 1636 cm^{-1} (arrows) indicate a predominant α-helix conformation, as well as a minor β-turn conformation, for Ala^{8}. (C) SP-B_{1-25} (A11) is the solid line and native SP-B_{1-25} is the dashed line. The minor peak at 1620 cm^{-1} in the SP-B_{1-25} (A11) spectrum indicates an α-helical conformation for Ala^{11}. (D) SP-B_{1-25} spectrum (dashed line in C) from SP-B_{1-25} (A11) (solid line in C). The peak at 1620 cm^{-1} (arrow) indicates an α-helix for Ala^{11}. See Table 2 for amino acid sequences of peptides. Spectra and peak assignments are representative of three independent experiments.

analyses about the intrinsic absorptions of secondary structures. It is of interest, then, that the proportions of secondary conformation determined by Fourier self-deconvolution are in good agreement with those obtained from site-directed ^{13}C-FTIR analysis (see above). Although our ^{13}C-FTIR findings support the use of Fourier self-deconvolution in this one instance, future comparisons should be performed on a much wider suite of proteins and peptides. Also, it should be emphasized that, unlike Fourier self-deconvolution, site-directed ^{13}C-FTIR measurements provide additional information on the actual location of secondary conformations.

The residue-specific, conformational model for SP-B_{1-25} in POPG lipid (Figs 6 and 10) may be further compared with previous models based on truncated SP-B_{1-25} peptides in membrane-mimic environments (33, 34). The local conformations for SP-B_{1-25} in POPG may be summarized as follows: β-sheet (residues 1–6), α-helix (residues 8–22) and random (residues 23–25). Using difference ^{13}C-FTIR spectroscopy of SP-B_{1-25} labeled with ^{13}C-carbonyl at single sites (Figs 8A, B and 9C, D), multiple conformations were also observed at each end of the α-helix (i.e. α-helix and β-turn for the Cys^{8} position, random and β-turn for Ala^{20}; see Fig. 6); this demonstrates some fraying of the helix at the N- and C-termini. Additional conformational flexibility was noted in the β-sheet of residues 1–6, from examination of the conformers determined with energy minimization (Fig. 10A). Earlier physical measurements with truncated peptides (33, 34) confirm this overall pattern of secondary structure in SP-B_{1-25}. For example, prior CD and conventional ^{12}C-FTIR spectroscopy on truncated SP-B_{1-25} peptides (e.g. SP-B_{1-9} and SP-B_{8-25}) in structure-promoting methanol, indicated elevated β-conformations in the N-terminal segment Phe^{1} to Cys^{8}, with high α-helix in the C-terminal segment Cys^{8} to Gly^{25} (33). Moreover, 2D-NMR analysis of another shortened N-terminal peptide (SP-B_{11-25}) in methanol or SDS demonstrated α-helix for residues 14–21 (34). Although these physical studies with shortened peptides support the present ^{13}C-FTIR results that the β-sheet localizes in the N-terminal portion and the α-helix in the C-terminal region, the two approaches show differences in the precise location of the major secondary elements. These

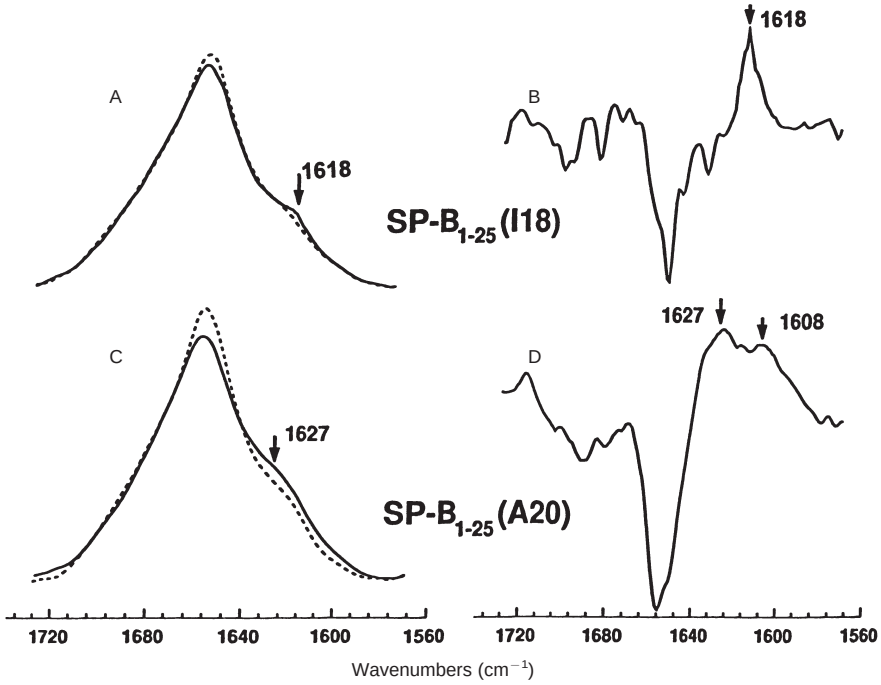

Figure 9. FTIR and difference FTIR spectra of the amide I band for ^{12}C-carbonyl SP-B_{1-25} (native) and single ^{13}C-carbonyl enhanced SP-B_{1-25} peptides labeled at Ile^{18} [i.e. SP-B_{1-25} (I18)] or Ala^{20} [i.e. SP-B_{1-25} (A20)]. Peptides at an initial P/L ratio of 1:70 were added to POPG liposomes suspended in PBS, pH 7.4. Spectra were recorded at 25°C on chromatographed peptide/liposomes that were dried on the ATR and hydrated with D_2O for 2 h. (A) SP-B_{1-25} (I18) is the solid line and native SP-B_{1-25} is the dashed line. The minor peak at 1618 cm^{-1} in the SP-B_{1-25} (I18) spectrum indicates an α-helix contribution for Ile^{18}. (B) SP-B_{1-25} spectrum (dashed line in A) from SP-B_{1-25} (I18) (solid line in A). The peak at 1618 cm^{-1} indicates an α-helix for Ile^{18}. (C) SP-B_{1-25} (A20) is the solid line and native SP-B_{1-25} is the dashed line. The minor peak at 1627 cm^{-1} in the SP-B_{1-25} (A20) spectrum indicates a β-turn conformation for Ala^{20}. (D) SP-B_{1-25} spectrum (dashed line in C) from SP-B_{1-25} (A20) (solid line in C). The peaks at 1627 and 1608 cm^{-1} (arrows) indicate that Ala^{20} exhibits both β-turn and random conformations; the loss of some symmetry for the negative and positive bands in (D) is attributed to a relatively high noise, which distorted the shape of the negative band. See Table 2 for amino acid sequences of peptides. Spectra and peak assignments are representative of three independent experiments.

discrepancies are attributed to the inherent uncertainties of working with truncated peptides that may fray at their unprotected N-terminal and C-terminal ends. Accurate assignment of SP-B_{1-25} conformations using truncated peptides requires that the fragments retain the same conformation as in the full-length peptide, and this is probably valid only as a first approximation. The conformation model developed here for SP-B_{1-25} in POPG lipid using ^{13}C-FTIR spectroscopy and energy minimizations (Figs 6 and 10) is more accurate because measurements are made using the full-length SP-B_{1-25} peptide containing nonperturbing, ^{13}C-carbonyl substituted amino acids. Moreover, ^{13}C-FTIR spectroscopy permits direct conformational measurements for peptide in actual membrane lipids, whereas the above studies with truncated peptides were performed using only membrane mimics (e.g. methanol and SDS).

It is worthwhile determining whether our structural motif for SP-B_{1-25} (Figs 6 and 10) is also represented in the corresponding domains of homologous proteins. As noted above, sequence and structural homologies indicate that the 79-residue, full-length SP-B probably assumes a 'saposin-fold', characterized by amphipathic α-helices forming a core stabilized by multiple intramolecular disulfide bonds (13–15, 21). The structural homologies for SP-B and other saposins may extend beyond the overall folding pattern to the local domain elements. For example, the N-terminal segment of SP-B_{1-25} (residues 1–9), with multiple proline residues interspersed with hydrophobic residues, exhibits striking sequence similarities with the corresponding region of hemerythrin (13). It should be noted, then, that the N-terminal domains of SP-B_{1-25} (residues 1–6; Figs 6 and 10) and hemerythrin (residues 1–9) (13, 20) each form β-sheet conformations. However, X-ray crystallographic analysis of hemerythrin (20) indicates that the N-terminal domain (residues 1–9) folds as an antiparallel β-sheet, whereas molecular modeling of the corresponding N-terminal region of SP-B_{1-25} (residues 1–6) shows an extended β-sheet with considerable flexibility, but only limited ability to form an antiparallel conformation. The N-terminal segment of SP-B_{1-25} (residues 1–9) was earlier proposed to act as a sort of

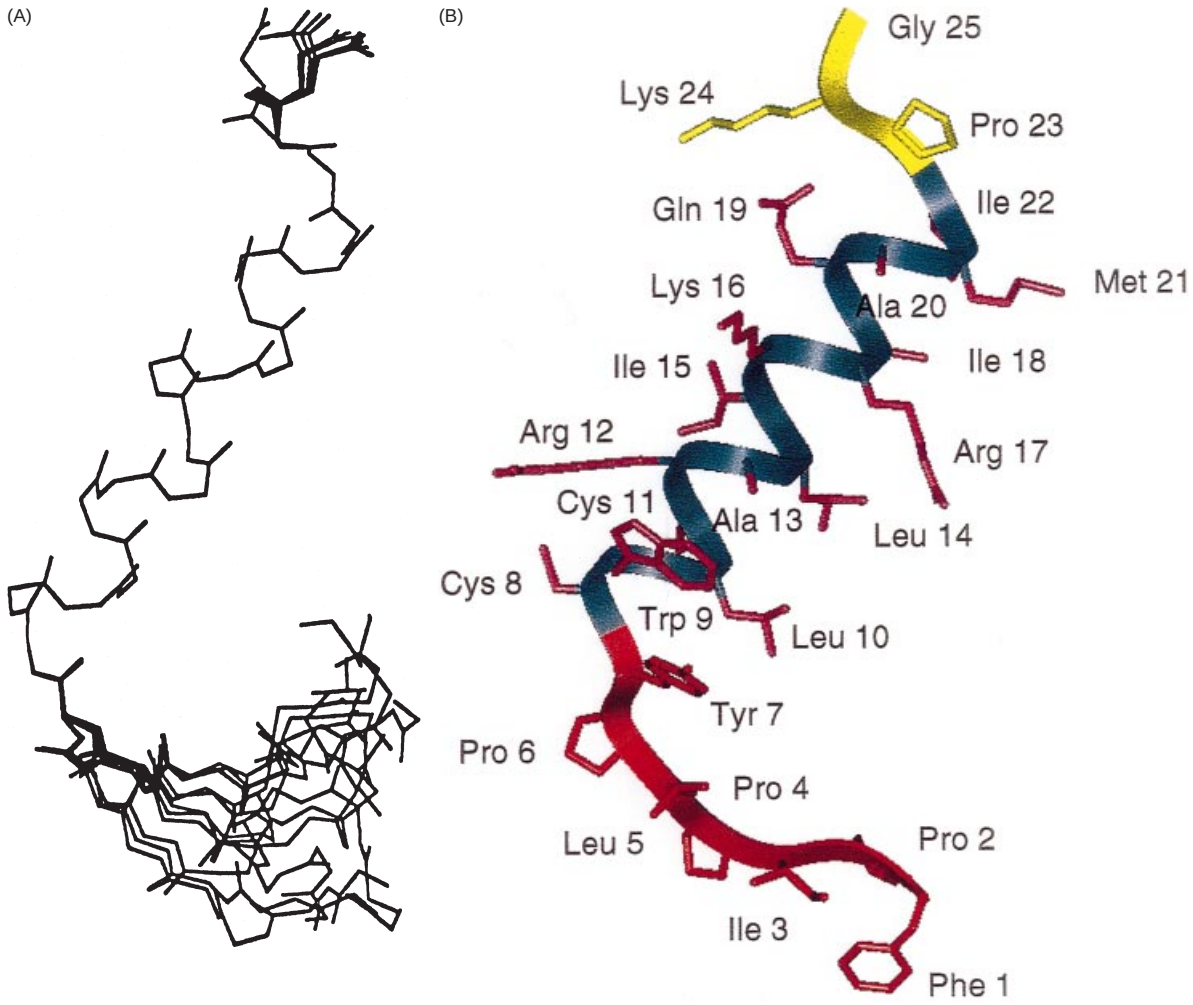

Figure 10. Conformation dynamic model (A) and ribbon representation (B) of the N-terminal peptide of human surfactant protein B ($SP\text{-}B_{1-25}$) in POPG liposomes. (A) Superimposed view of 10 solution structures of $SP\text{-}B_{1-25}$, calculated from simulated annealing, molecular dynamics and geometry optimization experiments. Constraints were imposed incorporating residue-specific information derived from FTIR spectroscopy of ^{13}C-labeled $SP\text{-}B_{1-25}$ peptides in POPG liposomes, suspended in PBS, pH 7.4. (B) Ribbon representation of a selected conformer showing the location of each residue, with the same orientation as in (A). Residues 8–22 encompass the α-helix (backbone shown as a blue ribbon and side-chains in red), while residues 1–7 are β-sheet (backbone shown as a red ribbon and side-chains in red) and residues 23–25 are random (backbone and side-chains shown in yellow).

'biochemical Velcro®,' facilitating *in vivo* either the aggregation of SP-B or the interactions of SP-B with surfactant protein C (SP-C) (30). The self-association of SP-B molecules forms protein-rich networks in lipids that may well be critical in mediating the surfactant activity of this protein (23, 26, 59). Our structural model for $SP\text{-}B_{1-25}$ (Fig. 10) raises the possibility that SP-B molecules cross-link through complementary hydrogen bonding of opposing N-terminal segments, each assuming an extended β-sheet conformation.

The α-helix observed here for $SP\text{-}B_{1-25}$ (residues 8–22) (Figs 6 and 10) is probably a ubiquitous feature in the N-terminal region of proteins sharing the 'saposin-fold.' The 3D structure of NK-lysin has been elucidated in a recent 2D-NMR study, and established an overall saposin folding pattern for the soluble protein (21). Based on the known sequence similarities between SP-B and NK-lysin and the 2D-NMR spectral finding of an α-helix for the N-terminus (residues 3–18) of NK-lysin, Liepinsh *et al.* (21) predicted that residues 7–22 of SP-B would also assume an α-helical conformation. Our experimental ^{13}C-FTIR results indicating α-helix for residues 8–22 of $SP\text{-}B_{1-25}$ (Figs 6 and 10) provide dramatic confirmation of this prediction and further suggest α-helical conformations for the corresponding N-terminal domains of other saposin proteins, such as saposins A–D, sulfated glycoprotein-I, acid sphingomyelinase, acyloxyacyl hydrolase and *E. histolytica* pore-forming peptides (amoebapores) (10, 13–15, 19, 21). Although the functional role of this N-terminal α-helical domain remains to be determined in other saposin proteins, prior work has established that this amphipathic α-helical motif is an important participant in the surfactant activities of $SP\text{-}B_{1-25}$ (24, 25, 32).

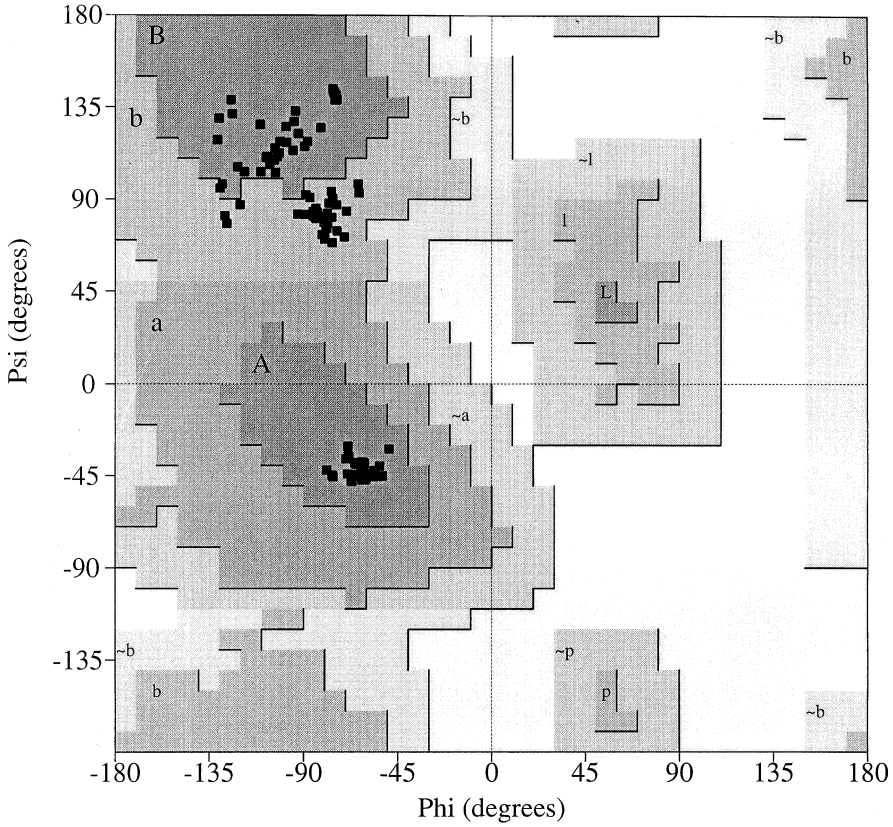

Figure 11. Ramachandran plot (54) for the 10 best structures of the N-terminal peptide of human surfactant protein B (SP-B_{1-25}), derived from the simulated annealing experiments. Psi (torsional angle for the C_a–C bond axis) is plotted vs. phi (torsional angle for the C_a–N bond axis). Initial constraints were obtained from residue-specific structural information derived from FTIR spectroscopy of ^{13}C-enhanced SP-B_{1-25} peptides suspended in POPG liposomes with PBS, pH 7.4. The dark areas represent most favored regions (A, B, L), while the light gray areas (a, b, l, p) and lightest gray areas (~a, ~b, ~l, ~p) represent additional allowed regions. Triangles denote glycine residues.

The results obtained here on SP-B_{1-25} confirm that the joint use of ^{13}C-FTIR spectroscopy and energy minimizations will be of general utility in mapping the secondary structures of conformationally heterogeneous peptides and proteins. Past ^{13}C-FTIR spectroscopic investigations have identified the sites of random, β-strand and β-turn structural domains in a soluble peptide (35), and also α-helical structure at specific regions in the transmembrane domain of phospholamban (36). Here, the residue-specific structure of the conformationally rich SP-B_{1-25} peptide bound to lipids has been elucidated using ^{13}C-FTIR spectroscopy and molecular simulations, such that the discrete locations of α-helix, β-sheet, random conformations have been characterized (Fig. 10). Furthermore, FTIR spectroscopic analysis of peptides substituted at single residues with ^{13}C-labeled carbonyls offers the potential to assess those conformationally flexible amino acids that assume multiple secondary structures (Fig. 6). We anticipate that future ^{13}C-FTIR spectroscopic and molecular modeling experiments may well yield complete conformational maps for other membrane-bound proteins (or peptides), which have been difficult to analyze with more standard methodologies (i.e. X-ray crystallographic and 2D-NMR spectroscopy). In future ^{13}C-FTIR spectroscopic investigations, it would be worthwhile studying whether the conformational properties of the SP-B_{1-25} peptide are the same as when this sequence is part of the full-length SP-B protein. Despite the similar surfactant activities reported for SP-B_{1-25} and full-length SP-B (22, 23, 26, 37, 59), it is unclear whether the isolated SP-B_{1-25} peptide accurately represents the structure of this domain in the full-length protein (10). This problem may be addressed by repeating the ^{13}C-FTIR experiments presented here with our ^{13}C-labeled SP-B_{1-25} peptides, each incorporated into the full-length (i.e. 79-residue), synthetic SP-B molecule (23, 59).

Acknowledgments: We thank Dr J. Bowie (UCLA) for the use of the AVIV 62DS spectropolarimeter and Dr C. Knobler (UCLA) for use of the dynamic light scattering device. The City of Hope Molecular Modeling Core Facility was supported by Cancer Center Support Grant P30 CA33572. This study was supported by National Institutes of Health grants HL 55534 (LMG, AJW, FJW) and HL 51177 (MML, JAZ). JAZ and AJW were also supported by Tobacco Related Disease Research Program grant 8RT-0077. KYCL was supported by the American Lung Association (RG-085-N), the March of Dimes Basil O'Connor Starter Research Award (5-FY98-0728), the David and Lucile Packard Foundation (99-1465), and the Searle Scholar Program/the Chicago Community Trust (99-C-105). The Drew ABI 431A peptide synthesizer was acquired with National Institutes of Health grant GM 50483 (AJW, LMG). IR structural data acquisition and analysis was supported by the Drew RCMI Bioinformatics Core (NCRR/RCMI G12 RR 03026).

References

1 Possmayer, F. (1988) A proposed nomenclature for pulmonary surfactant-associated proteins. *Am. Rev. Respir. Dis.* **138**, 990–998.

2 Power, J.H., Doyle, I.R., Davidson, K. & Nicholas, T.E. (1999) Ultrastructural and protein analysis of surfactant in the Australian lungfish *Neoceratodus forsteri* evidence for conservation of composition for 300 million years. *J. Exp. Biol.* **202**, 2543–2550.

3 Nogee, L.M., deMello, D.E., Dehner, L.P. & Colten, H.R. (1993) Pulmonary surfactant protein B deficiency in congenital pulmonary alveolar proteinosis. *N. Engl. J. Med.* **328**, 406–410.

4 Clark, J.C., Wert, S.E., Bachurski, C.J., Stahlman, M.T., Stripp, B.R., Weaver, T.E. & Whitsett, J.A. (1995) Targeted disruption of the surfactant protein B gene disrupts surfactant homeostasis, causing respiratory failure in newborn mice. *Proc. Natl Acad. Sci. USA* **92**, 7794–7798.

5 Walther, F.J., Hernandez-Juviel, J., Bruni, R. & Waring, A.J. (1998) Protein composition of synthetic surfactant affects gas exchange in surfactant-deficient rats. *Pediatr. Res.* **43**, 666–673.

6 Waring, A.J., Taeusch, H.W., Bruni, R., Amirkhanian, J.D., Fan, B.R., Stevens, R. & Young, J. (1989) Synthetic amphipathic sequences of surfactant protein-B mimic several physicochemical and *in vivo* properties of native pulmonary surfactant proteins. *Peptide Res.* **2**, 308–313.

7 Kaser, M.R. & Skouteris, G.G. (1997) Inhibition of bacterial growth by synthetic SP-B1-78 peptides. *Peptides* **18**, 1441–1444.

8 Baatz, J.E., Zou, Y. & Flume, P.A. (1999) Bacterial activity and SP-B profile of pulmonary surfactant from patients with cystic fibrosis. *Am. J. Resp. Crit. Care Med.* **159**, A895.

9 Van Golde, L.M.G. (1995) Potential role of surfactant proteins A and D in innate lung defense against pathogens. *Biol. Neonate* **67** (Suppl. 1), 2–17.

10. Hawgood, S., Derrick, M. & Poulain, F.R. (1998) Structure and properties of surfactant protein B. *Biochim. Biophys. Acta* **1408**, 150–160.

11. Folch, J., Lees, M. & Sloane Stanley, G.H. (1957) A simple method for the isolation and purification of total lipids from animal tissues. *J. Biol. Chem.* **226**, 497–509.

12. Johansson, J., Curstedt, T. & Jörnvall, H. (1991) Surfactant protein B: disulfide bridges, structural properties, and kringle similarities. *Biochemistry* **30**, 6917–6921.

13. Munford, R.S., Sheppard, P.O. & O'Hara, P.J. (1995) Saposin-like proteins (SAPLIP) carry out diverse functions on a common backbone structure. *J. Lipid Res.* **36**, 1653–1663.

14. Andersson, M., Curstedt, T., Jörnvall, H. & Johansson, J. (1995) An amphipathic helical motif common to tumourolytic polypeptide NK-lysin and pulmonary surfactant polypeptide SP-B. *FEBS Lett.* **362**, 328–332.

15. Dandekar, T. & Leippe, M. (1998) Molecular modeling of amoebapore and NK-lysin: a four-α-helix bundle motif of cytolytic peptides from distantly related organisms. *Fold. Design* **2**, 47–52.

16. Vandenbussche, G., Clercx, A., Clercx, M., Curstedt, T., Johansson, J., Jörnvall, H. & Ruysschaert, J.-M. (1992) Secondary structure and orientation of the surfactant protein B SP-B in a lipid environment. A Fourier transform infrared spectroscopy study. *Biochemistry* **31**, 9169–9176.

17. Oosterlaken-Dijksterhuis, M.A., Haagsman, H.P., Van Golde, L.M.G. & Demel, R.A. (1991) Characterization of lipid insertion into monomolecular layers mediated by lung surfactant proteins SP-B and SP-C. *Biochemistry* **30**, 10965–10971.

18. Pastrana-Rios, B., Taneva, S., Keough, K.M., Mautone, A.J. & Mendelsohn, R. (1995) External reflection absorption infrared spectroscopy study of lung surfactant proteins SP-B and SP-C in phospholipid monolayers at the air/water interface. *Biophys. J.* **69**, 2531–2540.

19. Waring, A.J., Chen, Y., Faull, K.F., Stevens, R., Sherman, M.A. & Fluharty, A.L. (1998) Porcine cerebroside sulfate activator (Saposin B) secondary structure: CD, FTIR, and NMR studies. *Mol. Genet. Metab.* **63**, 14–25.

20. Holmes, M.A. & Stenkamp, R.E. (1991) Structures of Met and Azidomet hemerythrin at 1.66 Å resolution. *J. Mol. Biol.* **220**, 723–737.

21. Liepinsh, E., Andersson, M., Ruysschaert, J.-M. & Otting, G. (1997) Saposin fold revealed by the NMR structure of NK-lysin. *Nat. Struct. Biol.* **4**, 793–795.

22. Longo, M.L., Bisagno, A.M., Zasadzinski, J.A.N., Bruni, R. & Waring, A.J. (1993) A function of lung surfactant protein SP-B. *Science* **261**, 453–456.

23. Lipp, M.M., Lee, K.Y.C., Zasadzinski, J.A.N. & Waring, A.J. (1996) Phase and morphology changes in lipid monolayers induced by SP-B protein and its amino-terminal peptide. *Science* **273**, 1196–1199.

24. Bruni, R., Taeusch, H.W. & Waring, A.J. (1991) Surfactant protein SP-B: lipid interactions of synthetic peptides representing the amino terminal amphipathic domain. *Proc. Natl Acad. Sci. USA* **88**, 7451–7455.

25. Fan, B.R., Bruni, R., Taeusch, H.W., Findlay, R. & Waring, A.J. (1991) Antibodies against synthetic amphipathic helical sequences of surfactant protein SP-B detect a conformational change in the native protein. *FEBS Lett.* **282**, 220–224.

26. Lipp, M.M., Lee, K.Y.C., Takamoto, D.Y., Zasadzinski, J.A.N. & Waring, A.J. (1998) Coexistence of buckled and flat monolayers. *Phys Rev. Lett.* **81**, 1650–1653.

27. Longmuir, K.J., Waring, A.J. & Haynes, S. (1992) Lipid bilayer fusion promoted by a synthetic N-terminal segment of surfactant protein B. *Biophys. J.* **61**, 2873–2873.

28. Oosterlaken-Dijksterhuis, M.A., Van Eijk, M., Van Golde, L.M.G. & Haagsman, H.P. (1992) Lipid mixing is mediated by the hydrophobic surfactant protein SP-B but not by SP-C. *Biochim. Biophys. Acta* **1110**, 45–50.

29. Poulain, F.R., Nir, S. & Hawgood, S. (1996) Kinetics of phospholipid membrane fusion induced by surfactant apoproteins A and B. *Biochim. Biophys. Acta* **1278**, 169–175.

30. Pérez-Gil, J. & Keough, K.M.W. (1991) Identical and similar amino acid sequences in the pulmonary surfactant proteins SP-B and SP-C and hemerythrin and myohemerythrin – an example of 'biochemical Velcro'? *Biochem. Int.* **25**, 715–721.

31. Takahashi, A., Waring, A.J., Amirkhanian, J.D., Fan, B.R. & Taeusch, H.W. (1990) Structure–function relationships of bovine pulmonary surfactant proteins: SP-B and SP-C. *Biochim. Biophys. Acta* **1044**, 43–49.

32. Waring, A.J., Gordon, L.M., Taeusch, H.W. & Bruni, R. (1993) Amphipathic helical segments in lung surfactant proteins. In: *The Amphipathic Helix* (Epand, R.M., ed.) CRC Press, Inc., Boca Raton, FL, pp.143–171.

33. Gordon, L.M., Horvath, S., Longo, M.L., Zasadzinski, J.A.N., Taeusch, W., Faull, K., Leung, C. & Waring, A.J. (1996) Conformation and molecular topography of the N-terminal segment of surfactant protein B in structure-promoting environments. *Protein Sci.* **5**, 1662–1675.

34. Kumar, S. (1994) Conformational analysis of a synthetic fragment of lung surfactant apolipoprotein b. Thesis, University of Minnesota, Minneapolis, MN.

35. Tadesse, L., Nazarbaghi, R. & Walters, L. (1991) Isotopically enhanced infrared spectroscopy: a novel method for examining secondary structure at specific sites in conformationally heterogeneous peptides. *J. Am. Chem. Soc.* **113**, 7036–7037.
36. Ludlam, C.F.C., Arkin, I.T., Liu, X.-M., Rothman, M.S., Rath, P., Aimoto, S., Smith, S.O., Engelman, D.M. & Rothschild, K.J. (1996) Fourier transform infrared spectroscopy and site-directed isotope labeling as a probe of local secondary structure in the transmembrane domain of phospholamban. *Biophys. J.* **70**, 1728–1736.
37. Longo, M.L., Waring, A.J. & Zasadzinski, J.A.N. (1992) Lipid bilayer surface association of lung surfactant protein SP-B, amphipathic segment detected by flow immunofluorescence. *Biophys. J.* **63**, 760–773.
38. Eisenberg, D. & Wesson, M. (1990) The most highly amphipathic alpha helices include two amino acid segments in human immunodeficiency virus glycoprotein gp41. *Biopolymers* **29**, 171–177.
39. Waring, A.J., Harwig, S.S.L. & Lehrer, R.I. (1996) Structure and activity of protegrin-1 in model lipid membranes. *Protein Peptide Lett.* **3**, 177–184.
40. Longo, M.L., Waring, A.J., Gordon, L.M. & Hammer, D.A. (1998) Area expansion and permeation of phospholipid membrane bilayers by influenza fusion peptides and melittin. *Langmuir* **14**, 2385–2395.
41. Waring, A.J., Faull, K.F., Leung, C., Chang-Chien, A., Mercado, P., Taeusch, H.W. & Gordon, L.M. (1996) Synthesis, secondary structure and folding of the bend region of lung surfactant protein B. *Peptide Res.* **9**, 28–39.
42. Johnson, W.C.J. (1990) Protein secondary structure and circular dichroism: a practical guide. *Proteins: Struct. Func. Genet.* **7**, 205–214.
43. Chen, Y.H., Yang, J.T. & Chau, K.H. (1974) Determination of the helix and β form of proteins in aqueous solution by circular dichroism. *Biochemistry* **13**, 3350–3359.
44. Mobley, P.W., Waring, A.J., Sherman, M.A. & Gordon, L.M. (1999) Membrane interactions of the synthetic N-terminal peptide of HIV-1 gp41 and its structural analogs. *Biochim. Biophys. Acta* **1418**, 1–18.
45. Martin, I., Defrise-Quertain, F., Decroly, E., Vandenbranden, M., Brasseur, R. & Ruysschaert, J.-M. (1993) Orientation and structure of the NH_2-terminal HIV-1 gp41 peptide in fused and aggregated liposomes. *Biochim. Biophys. Acta* **1145**, 124–133.
46. Kauppine, J., Moffatt, D., Mantsch, H. & Cameron, D. (1981) Fourier self-deconvolution: a method for resolving intrinsically overlapped bands. *Appl. Spectrosc.* **35**, 272–278.
47. Byler, D.M. & Susi, H. (1986) Examination of the secondary structure of protein by deconvolved FTIR spectra. *Biopolymers* **25**, 469–487.
48. Surewicz, W.K. & Mantsch, H.H. (1988) New insight into protein secondary structure from resolution-enhanced infrared spectra. *Biochim. Biophys. Acta* **952**, 115–130.
49. Goormaghtigh, E., Cabiaux, V. & Ruysschaert, J.-M. (1990) Secondary structure and dosage of soluble and membrane proteins by attenuated total reflection Fourier-transform infrared spectroscopy on hydrated films. *Eur. J. Biochem.* **193**, 409–420.
50. Dwivedi, A.M. & Krimm, S. (1984) Vibrational analysis of peptides, polypeptides, and proteins. XVIII. Conformational sensitivity of the α-helix spectrum: a_I and α_{II}-poly (L-alanine). *Biopolymers* **23**, 923–943.
51. Haris, P.I., Robillard, G.T., van Dijk, A.A. & Chapman, D. (1992) Potential of ^{13}C and ^{15}N labeling for studying protein–protein interactions using Fourier transform infrared spectroscopy. *Biochemistry* **31**, 6279–6284.
52. Dauber-Osguthorpe, P., Roberts, V.A., Osguthorpe, D.J., Wolff, J., Genest, M. & Hagler, A.T. (1988) Structure and energetics of ligand binding to proteins: *Escherichia coli* dihydrofolate reductase-trimethoprim, a drug-receptor system. *Proteins: Struct. Func. Genet.* **4**, 31–47.
53. Maple, J.R., Dinur, U. & Hagler, A.T. (1988) Derivation of force fields for molecular mechanics and dynamics from *ab initio* energy surfaces. *Proc. Natl Acad. Sci. USA* **85**, 5350–5354.
54. Laskowski, R.A., MacArthur, M., Moss, D.S. & Thornton, J.M. (1993) PROCHECK: a program to check the stereochemical quality of protein structures. *J. Appl. Cryst.* **26**, 283–291.
55. Gong, Y., Zhou, H.X., Guo, M. & Kallenbach, N.R. (1995) Structural analysis of the N- and C-termini in a peptide with a consensus sequence. *Protein Sci.* **4**, 1446–1456.
56. Padmanabhan, S., Jimenez, M.A., Laurents, D.V. & Rico, M. (1998) Helix-stabilizing nonpolar interactions between tyrosine and leucine in aqueous and TFE solutions: 2D-^1H NMR and CD studies in alanine-lysine peptides. *Biochemistry* **37**, 17318–17330.
57. Okamura, E., Umemura, J. & Takenaka, T. (1990) Orientation studies of hydrated dipalmitoylphosphatidylcholine multilayers by polarized FTIR-ATR spectroscopy. *Biochim. Biophys. Acta* **1025**, 94–98.
58. Goormaghtigh, E., De Meutter, J., Vanloo, B., Brasseur, R., Rosseneu, M. & Ruysschaert, J.-M. (1989) Evaluation of the secondary structure of apoB-100 in low-density lipoprotein (LDL) by infrared spectroscopy. *Biochim. Biophys. Acta* **1006**, 147–150.
59. Lee, K.Y.C., Lipp, M.M., Zasadzinski, J.A.N. & Waring, A.J. (1997) Effects of lung surfactant specific protein SP-B and model SP-B peptide on lipid monolayers at the air–water interface. *Colloids Surfaces A: Physicochem. Eng. Aspects* **128**, 225–242.